Atmos. Chem. Phys., 25, 17275–17300, 2025
https://doi.org/10.5194/acp-25-17275-2025

Atmospheric Chemistry and Physics
Open Access
EGU

Research article

Optimizing CCN predictions through inferred modal aerosol composition – a boreal forest case study

Rahul Ranjan[1,2], **Maura Dewey**[4,2], **Liine Heikkinen**[1,2], **Lauri R. Ahonen**[3], **Krista Luoma**[3,6], **Paul Bowen**[5], **Tuukka Petäjä**[3], **Annica M. L. Ekman**[4,2], **Daniel G. Partridge**[5], and **Ilona Riipinen**[1,2]

[1]Department of Environmental Science (ACES), Stockholm University, 10691, Stockholm, Sweden
[2]Bolin Centre for Climate Research, Stockholm University, 10691, Stockholm, Sweden
[3]Institute for Atmospheric and Earth System Research/Physics, University of Helsinki, 00014, Helsinki, Finland
[4]Department of Meteorology, Stockholm University, Stockholm, Sweden
[5]Department of Mathematics and Statistics, Faculty of Environment, Science and Economy, University of Exeter, EX4 4QF, Exeter, United Kingdom
[6]Atmospheric Composition Research, Finnish Meteorological Institute, Helsinki, 00560, Finland

Correspondence: Rahul Ranjan (rahul.ranjan@aces.su.se) and Ilona Riipinen (ilona.riipinen@aces.su.se)

Received: 11 April 2025 – Discussion started: 8 May 2025
Revised: 13 October 2025 – Accepted: 14 October 2025 – Published: 2 December 2025

Abstract. The contribution of natural aerosol particles from boreal forests to total aerosol loadings may increase with reduction in anthropogenic emissions. Aitken and accumulation mode particles in boreal regions differ significantly in hygroscopicity, and ignoring this size dependence can cause large uncertainty in Cloud Condensation Nuclei (CCN) prediction. We applied κ-Köhler theory to a multi-year dataset (2016–2020) from Hyytiälä, Finland, to evaluate different representations of aerosol chemical composition for CCN prediction. Overpredictions by forward closures using either bulk chemical composition from an Aerosol Chemical Speciation Monitor (ACSM) or a constant $\kappa = 0.18$ were mitigated to a great extent by optimizing size-resolved composition using two inverse modeling approaches: (1) Nelder–Mead method with the size distribution fixed to its median during each 2 h CCN measurement cycle, and (2) MCMC (Markov Chain Monte Carlo) accounting also for the variability in the size distribution during each cycle. Both methods improved closure at SS = 0.2 %–1.0 % (with Geometric Mean Bias GMB values 1.12–1.20 and 0.95–1.05, respectively), with moderate improvement at 0.1 % (GMBs of 1.53 and 1.32, respectively). The Aitken mode was enriched in organics in 77 % of cases using method (1) and 46 % using method (2) – with typical κ values of ~ 0.1 for Aitken and ~ 0.3 for accumulation modes. The results generally align with known size-dependent chemical composition in Hyytiälä and indicate that variability in CCN hygroscopicity is largely driven by Aitken mode composition. Our results demonstrate the potential of inverse CCN closure methods for obtaining valuable information of the size-dependent chemical composition.

1 Introduction

Aerosol particles play a critical role in the formation of cloud droplets. They serve as cloud condensation nuclei (CCN) by lowering the energy barrier for heterogeneous nucleation of water, thus promoting cloud droplet activation at atmospheric levels of water vapor supersaturations SS (Köhler 1936; Pruppacher and Klett, 2010). The subset of aerosol particles that act as CCN affects the cloud droplet number concentration (CDNC), thus changes in the CCN concentration (N_{CCN}) may modulate cloud radiative properties and lifetime – phenomena known as the first (Twomey, 1974) and second (Albrecht, 1989) indirect aerosol climate effects. The parameterization schemes related to cloud droplet formation in global climate models (e.g., Abdul-Razzak and Ghan, 2000, 2002; Nenes and Seinfeld, 2003; Fountoukis and Nenes, 2005; Barahona et al., 2010; Betancourt and Nenes, 2014) rely on estimates of CCN concentrations which are calculated based on simplified treatment of aerosol size distributions, chemical compositions and the Köhler theory, leading to varying degrees of uncertainty depending on the specific scheme used (Simpson et al., 2014). Enhanced understanding of aerosol particles and their role as CCN may be used to improve representations of aerosol-cloud interactions (ACI) in global climate models, which remain a significant source of uncertainty in estimates of total anthropogenic radiative forcing over the industrial period (IPCC, 2023; Seinfeld et al., 2016).

N_{CCN} and CDNC are primarily determined by aerosol properties and the drivers of maximum supersaturation ($\mathrm{SS}_{\mathrm{max}}$) fluctuations (e.g. updraft velocities, radiative cooling rates, water vapor concentration field see e.g. Köhler, 1936; Rogers and Yau, 1989; Reutter et al., 2009; Anttila et al., 2012; Partridge et al., 2012), both of which are known to display large spatial and temporal variability. Many studies have evaluated N_{CCN} predictions from Köhler theory against observations of aerosol particle size distributions, chemical composition and meteorological parameters in various environments. These investigations, often termed aerosol-CCN closure studies or hygroscopicity-CCN closure studies, will hereafter be referred as "closure studies". Typically, such studies have involved forward modeling, where observational input data (e.g., aerosol size distribution, composition, and hygroscopicity) is utilized to predict N_{CCN} using the Köhler theory. The model outputs are then compared directly with observed CCN data to assess consistency and evaluate the predictions (e.g., Bougiatioti et al., 2009; Martin et al., 2011; Rejano et al., 2024). In contrast, relatively few studies have leveraged inverse modeling frameworks, which use observed CCN data to infer the properties of the aerosol population or model parameters. In these approaches, CCN measurements are treated as a reference (while also accounting for observational uncertainty), and model parameters such as surface tension, hygroscopicity, and size distribution are adjusted to reproduce the observations. This not only enables the retrieval of aerosol population characteristics from CCN data but also provides a means to rigorously test model assumptions and quantify the influence of uncertain calibration parameters on predicted CCN concentrations (e.g., Partridge et al., 2011, 2012; Lowe et al., 2016). In this study we intend to use a CCN closure study as a means to infer information on the size-dependent chemical composition of CCN-sized aerosol particles, to enhance bulk chemical composition measurements.

Köhler theory (Köhler, 1936) has been widely used in earlier studies as the standard framework for predicting CCN activation and proved effective under most relevant atmospheric conditions, provided that there was accurate knowledge of the aerosol number size distribution, size-dependent chemical composition, and SS. To simplify the representation of aerosol hygroscopic growth and CCN activity, Petters and Kreidenweis (2007) introduced the non-dimensional hygroscopicity parameter κ, to facilitate comparisons of data sets with varying levels of detail for the aerosol chemical composition. These theoretical frameworks along with information about particle number size distributions and chemical composition are utilized to calculate the activation diameter (D_{act}) of the dry particles and finally the CCN concentration at a particular ambient SS. A successful closure study aims for the modelled CCN and measured CCN to be comparable within measurement uncertainties and is notably influenced by the accuracy of the relevant measurements and any theoretical approximations.

The aqueous phase thermodynamics of soluble inorganic salts like ammonium sulfate ($(NH_4)_2SO_4$), sodium chloride (NaCl), ammonium bisulfate (NH_4HSO_4) and ammonium nitrate (NH_4NO_3) are considered to be relatively well-understood (e.g., Zhang et al., 2000; Nenes et al., 1998, 1999), and yield accurate predictions of CCN activation of these compounds using Köhler theory. However, atmospheric aerosol particles also typically contain a significant organic mass fraction (Zhang et al., 2007), originating from various sources. In the atmosphere, organic aerosol typically forms a complex mixture with inorganic aerosol species. The organic component evolves over time modifying both the mass concentration and the properties of the aerosol (Robinson et al., 2007; Jimenez et al., 2009). Organic aerosol is comprised of a wide variety of molecules (e.g., Hallquist et al., 2009; Nozière et al., 2015; Ditto et al., 2018) with different properties, such as solubility, volatility and surface activity (e.g., Hodzic et al., 2014; Ye et al., 2016; Huang et al., 2024; El Haber et al., 2024). While many of the atmospheric organic compounds are water-soluble, their hygroscopicity is typically lower than that of inorganic salts (e.g., Pöhlker et al., 2023). Nevertheless, organic aerosol plays a significant role in determining (N_{CCN}) and CDNC, especially because organic aerosol formation drives aerosol particle growth towards CCN-relevant sizes in many environments (e.g., Riipinen et al., 2011; Mohr et al., 2019; Croft et al., 2019; Zheng et al., 2020; Qiao et al., 2021). Importantly, some organic aerosol properties beyond hygroscopicity such as solubility or surface activity, may enhance the likelihood of an Aitken mode aerosol particle to serve as CCN (Lowe et al., 2019). Historically, in studies where the organic aerosol contribution to the CCN activation was not adequately considered, errors of up to an order of magnitude were observed between predicted and measured N_{CCN} in many environments (e.g., Bigg, 1986; Covert et al., 1998; Chuang et al., 2000; Rissman et al., 2006; Quinn et al., 2008). This discrepancy highlights the need to include organics in CCN closure studies. Studies incorporating organic aerosol effects demonstrated significant improvements in closure as compared with attempts considering inorganics alone (e.g., Broekhuizen et al., 2006; Rose et al., 2008; Ervens et al., 2010; Gunthe et al., 2009; Bougiatioti et al., 2009; Jurányi et al., 2010; Siegel et al., 2022). These findings underscore the importance of organics in CCN prediction, particularly in air masses with substantial freshly emitted primary biogenic or anthropogenic organic vapors.

Boreal forests are environments where local biogenic emissions act as a major source of aerosol particles, with organic aerosol constituting 50 %–80 % of the observed sub-micron aerosol mass (Heikkinen et al., 2020). This dominance of organics results from the emission of biogenic volatile organic compounds (BVOCs) by the forests, which promotes secondary organic aerosol (SOA) production. Understanding the factors controlling N_{CCN} above boreal forests is necessary for constraining the magnitude of the climate feedbacks involving natural forest aerosols and clouds, which are likely to increase in importance as anthropogenic aerosol emissions decrease (see e.g., Paasonen et al., 2013; Yli-Juuti et al., 2021; Blichner et al., 2024).

Hämeri et al. (2001) utilized Hygroscopicity Tandem Differential Mobility Analyzers (HTDMAs) during the BIOFOR campaign at the SMEAR II Hyytiälä forest field station in south-central Finland, to measure the hygroscopic growth factors of aerosol particles at 90 % relative humidity (RH), and reported Aitken mode particles (with growth factors between 1.0 and 1.4) to be less hygroscopic than accumulation mode particles (growth factors ~ 1.6). Sihto et al. (2011) studied the annual cycles of aerosol hygroscopicity and CCN, finding the hygroscopicity at sub-saturated conditions to be a good predictor of the CCN activity as well. They concluded the average hygroscopicity parameter κ to be 0.18 (for SS values between 0.1 % and 1 % during July 2008 and June 2009) and therefore, the CCN-sized particles to be mostly organic, but to also contain more hygroscopic material such as ammonium sulfate (see also Cerully et al., 2011). Paramonov et al. (2013) used a size-segregated CCN observation data set collected between January 2009 and April 2012 from Hyytiälä, which revealed that the median κ exhibited significant variation depending on the SS and hence particle size. Specifically, the median κ was 0.41 at 0.1 % SS and 0.14 at 1.0 % SS. At 0.1 % SS, only the upper tail of the aerosol size distribution is activated, so the corresponding κ represents the largest particles in the distribution – indicating them to contain more inorganic species as compared with the smaller particles. In contrast, activation at 1.0 % SS includes smaller particles, which are generally more organic, resulting in a lower κ. The size-dependence of hygroscopicity was more pronounced during the winter months compared to the summer. In a follow-up study, Paramonov et al. (2015) identified a statistically significant difference in the hygroscopicity of Aitken and accumulation mode particles in northern locations and concluded that the assumption of a size-independent κ potentially leads to a recurring overestimation in CCN predictions at supersaturations above 0.6 % in the boreal environment. In the closure study by Schmale et al. (2018), predictions using bulk chemical composition data indeed led to an over-prediction (geometric mean bias of 1.32 at $SS = 0.5\,\%$) of N_{CCN} for the period between January 2012 and June 2014.

In large-scale atmospheric models, the aerosol size distribution is often represented by a number of log-normal modes, and N_{CCN} are estimated from SS_{max} based on dynamics (e.g., updraft) and physicochemical properties of the aerosol modes – as the abundance of particles with variable sizes and compositions influences the development of SS and hence the CCN activation (e.g., Abdul-Razzak and Ghan, 2000). A number of studies (e.g., Sihto et al., 2011; Paramonov et al., 2013; 2015; Bulatovic et al., 2021; Pöhlker et al., 2021; Lowe et al., 2019; Duplessis et al., 2024) have demonstrated that Aitken mode particles can contribute significantly to CDNC, particularly in clean conditions. Therefore, constraints on the physicochemical properties of both Aitken and accumulation mode particles are important for predictions of N_{CCN} and CDNC. Unfortunately, the standard methods used for measurements of aerosol chemical composition (e.g., Aerosol Chemical Speciation Monitor ACSM; see Sect. 2.1.4) cannot typically separate accumulation and Aitken mode composition. The few studies reporting size-segregated aerosol composition in forested environments suggest an enrichment of inorganics in the accumulation mode, and higher mass fractions of organics in the Aitken mode (Allan et al., 2006; Hao et al., 2013; Levin et al., 2014; Timonen et al., 2008; Saliba et al., 2020). Studies involving a full annual coverage suggest a more size-dependent composition in early spring and winter (Levin et al., 2014; Timonen et al., 2008) compared to the summer. These findings are also qualitatively in line with the studies investigating the growth of Aitken mode particles in Hyytiälä, explainable with organic condensation (e.g., Riipinen et al., 2011 Mohr et al., 2019). Campaign-wise studies like Cubison et al. (2008); Broekhuizen et al. (2006); Stroud et al. (2007); Meng et al. (2014) used size-resolved Aerosol Mass Spectrometer (AMS) data, which is typically sparse, to achieve CCN closure in different environments, demonstrating that size-dependent chemical composition of aerosol particles can often explain the apparent discrepancies between observed and predicted CCN concentrations. Taken together, these results suggest that observations of CCN concentrations have the potential to be used in an inverse manner to constrain Aitken and accumulation mode chemical compositions separately – if information on the particle size distribution and an estimate of the bulk chemical composition is available.

In this study, we employ long-term (2016–2020) concurrent measurements from the SMEAR II atmospheric monitoring site in the boreal forest (Hyytiälä, Finland) to perform inverse aerosol-CCN closures, where we optimize the modal aerosol chemical composition using two approaches: (1) assuming a fixed size distribution set to the median values during each CCN spectrum cycle applying a Nelder-Mead optimization method, and (2) allowing the size distribution parameters to vary within the observed variability during each cycle and using Markov Chain Monte Carlo simulations for finding the optimal size-dependent composition. Additionally, we test the performance of two forward closure approaches: a commonly used approach, which utilizes the bulk aerosol chemical composition (i.e., size-independent composition) observations ("bottom-up" approach) to estimate the κ and predict CCN concentrations, and a simpler approach using a constant hygroscopicity parameter κ of 0.18 throughout the study period, as recommended by Sihto et al. (2011). Specifically, our study aims to address the following questions:

1. How does the chosen representation of κ affect the CCN closure on a multi-year and seasonal basis?

2. To what degree can a forward CCN closure be achieved when assuming size-independent chemical composition?

3. Can we improve CCN closure by assuming mode-dependent composition while keeping the size distribution fixed to the observations?

4. Which modal chemical composition and associated hygroscopicity parameter (κ) provide a more accurate closure compared to using bulk chemical composition? Furthermore, how do the inferred modal chemical composition and κ values differ when the variability of the aerosol size distribution during the CCN cycle period is accounted for versus when it is neglected?

Through assuming that the SMEAR II station represents a remote continental site with a reasonable accuracy, we aim to provide useful insights on the role and dependencies of CCN loadings on natural aerosol properties.

2 Methods and data

Figure 1 provides an overview of the data and the overall approach used in this study. The core long-term data sets utilized were simultaneous observations of aerosol number size distribution between 3 and 1000 nm, chemical composition of the sub-micron (bulk) aerosol fraction and N_{CCN} at SS between 0.1 % and 1 % during the period of 2016–2020. κ-Köhler theory (Petters and Kreidenweis, 2007) was used to predict N_{CCN} based on the size distribution and composition data with three different approaches for estimating the hygroscopicity parameter κ: (1) κ_{bulk}, i.e. calculating κ using the observed bulk (size-independent) sub-micron aerosol composition; (2) $\kappa_{0.18}$, i.e. using a constant κ value of 0.18 (Sihto et al., 2011) for the entire observation period; and (3) κ_{opt} and κ_{MCMC} i.e. determining κ through an inverse closure assuming variable Aitken and accumulation mode compositions while maintaining the total sub-micron chemical composition as observed. In the following subsections we present further details on the measurement site and observations of aerosol number size distribution, sub-micron chemical composition, as well as concentrations of CCN at different supersaturations. Finally, a detailed description of methods including κ-Köhler theory and inverse closure is provided.

2.1 Experimental data

2.1.1 Station for Measuring Ecosystem–Atmosphere Relations (SMEAR II)

The SMEAR II measurement site at Hyytiälä is located at 61°51′ N, 24°17′ E, 181 m above sea level, and represents a boreal forest environment with some anthropogenic influence, particularly from the southern direction where many industrialized areas within Finland, Russia, and continental Europe are located (Patokoski et al., 2015; Riuttanen et al., 2013; Yttri et al., 2011; Tunved et al., 2006). The extent of the representativeness of SMEAR II for boreal forest environments varies seasonally and with air mass origin. The station is surrounded by mixed forest which covers 80 % of the land within a 5 km radius and 65 % within a 50 km radius (Williams et al., 2011). Primary local emission sources include a sawmill situated to the northeast and a pellet factory located around 6–7 km southeast of SMEAR II. Overall, the station can be considered a rural background site because the nearest major city, Tampere, is located about 60 km southeast of the measurement location. During the summer, local BVOC emissions (Hakola et al., 2012; Feijó Barreira et al., 2018), primarily those of monoterpenes, act as a major source of SOA at the station (Heikkinen et al., 2020; Heikkinen et al., 2021). New particle formation (NPF), which is an important process contributing to N_{CCN} globally (e.g., Merikanto et al., 2009), is commonly observed at SMEAR II, especially in spring and fall (Nieminen et al., 2014). Sulfuric acid, bases and low-volatility BVOC oxidation products (e.g., Kulmala et al., 2014; Lehtipalo et al., 2018; Yan et al., 2018), have been identified as critical precursors for NPF at the site. During the winter, aerosol particles observed at the site are mainly from long-range transport (Riuttanen et al., 2013) and are frequently cloud-processed (Isokääntä et al., 2022). During this season, aerosol particles contain a larger inorganic component (about 36 % as compared to 23 % in summer, Heikkinen et al., 2020) increasing their hygroscopicity. However, during the winters, the increased contribution of black carbon (about 15 % as compared to 6 % in summer, Luoma et al., 2021), a hydrophobic aerosol component, decreases the overall hygroscopicity of the particles. SMEAR II is unique due to the comprehensive set of long-term measurements, crucial for answering questions related to aerosol-cloud interactions, which have been conducted for several years (Kulmala, 2018). Although facilities for measuring aerosol size distribution and CCN have existed for a long time (since 1996 and 1998, respectively), long-term composition measurements have become available more recently (Luoma et al., 2021; Heikkinen et al., 2020). This

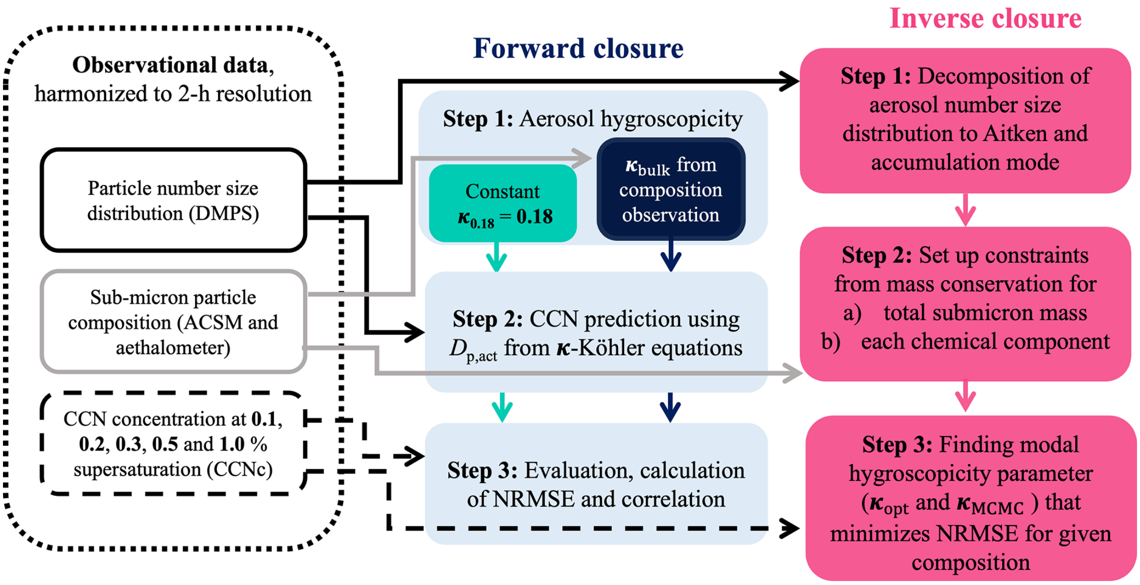

Figure 1. Workflow diagram of the observational data along with the steps made in its processing and analysis. NRMSE and $D_{p,act}$ refer to Normalized Root Mean Squared Error (see Sect. 2.2.4) and dry activation diameter respectively. DMPS refers to Differential Mobility Particle Sizer, ACSM to Aerosol Chemical Speciation Monitor, CCN to Cloud Condensation Nuclei and CCNc to Cloud Condensation Nuclei counter.

advancement has been due to the development and deployment of the ACSM and an aethalometer setup which provide near-real time data on the organics, sulfate, nitrate, ammonium, chloride and equivalent black carbon (eBC) in submicrometre aerosol particles (see also Sect. 2.1.4).

2.1.2 Aerosol number size distribution

At SMEAR II, a Differential mobility Particle Sizer (DMPS) has been used for particle number size distribution (PNSD) measurements in a size range from 3 to 1000 nm since 1996 (Aalto et al., 2001). The DMPS data has the time resolution of 10 min. The data used in this study were accessed from SmartSMEAR database (https://smear.avaa.csc.fi/download, last access: 28 April 2022) for years 2016–2020 (see Fig. 2a). Medians of the size distribution data were taken over the start and end time periods of the respective co-located CCN measurements (see Sect. 2.1.3).

The twin-DMPS system consists of two Vienna-type Differential Mobility Analyzers (DMAs), each designed to classify aerosol particles into size bins across two distinct size ranges: 3–40 and 20–1000 nm. The sizing is based on the electrical mobility of the sampled and charged aerosol particles. Air is sampled at a height of 8 m above ground level with a common aerosol inlet. The common inlet line has a diameter of 100 mm and a flow velocity of 0.5 m s^{-1}. The sample flow for the instruments is taken from the centreline. The aerosol flow rates in the DMAs are 4 and 1 L min^{-1}, respectively. The sheath flows, with flow rates of 20 and 5 L min^{-1}, are dried to maintain RH of less than 40 %, while the aerosol flows are not dried. The particle concentration following each DMA is measured using Condensation Particle Counters (CPCs). For small particles (3–40 nm), a TSI 3025 CPC model was utilized (later changed to model TSI3776 after October 2016), while a TSI 3750 CPC is used for the detection of the larger particles in the size range 20–1000 nm.

As a first step toward the inverse closure (see also Sect. 2.2.3), we applied a Python implementation (Khadir, 2023) of the modal-fitting algorithm described by Hussein et al. (2005) to decompose the measured aerosol size distributions into two modes. The algorithm takes size distribution as input and returns the lognormal parameters (number concentration, geometric standard deviation, geometric mean diameter GMD) of different modes as output. While the algorithm would allow fitting up to four modes, bimodal fits (Aitken and accumulation mode, respectively; Supplement Fig. S1a) were selected to avoid overfitting (see also Liwendahl, 2021). The bimodal fits enabled us to reproduce the aerosol size distributions with a high correlation (Pearson correlation coefficient $R = 0.99$) between the observed total particle number concentration and that calculated from the fitted parameters (Fig. S1b).

2.1.3 CCN concentrations

The time series of observed N_{CCN} were obtained using a CCN-100, a continuous-flow streamwise thermal-gradient CCN counter (CCNc), commercially provided by Droplet Measurement Technologies (Roberts and Nenes, 2005). The CCNc can be used in either monodisperse or polydis-

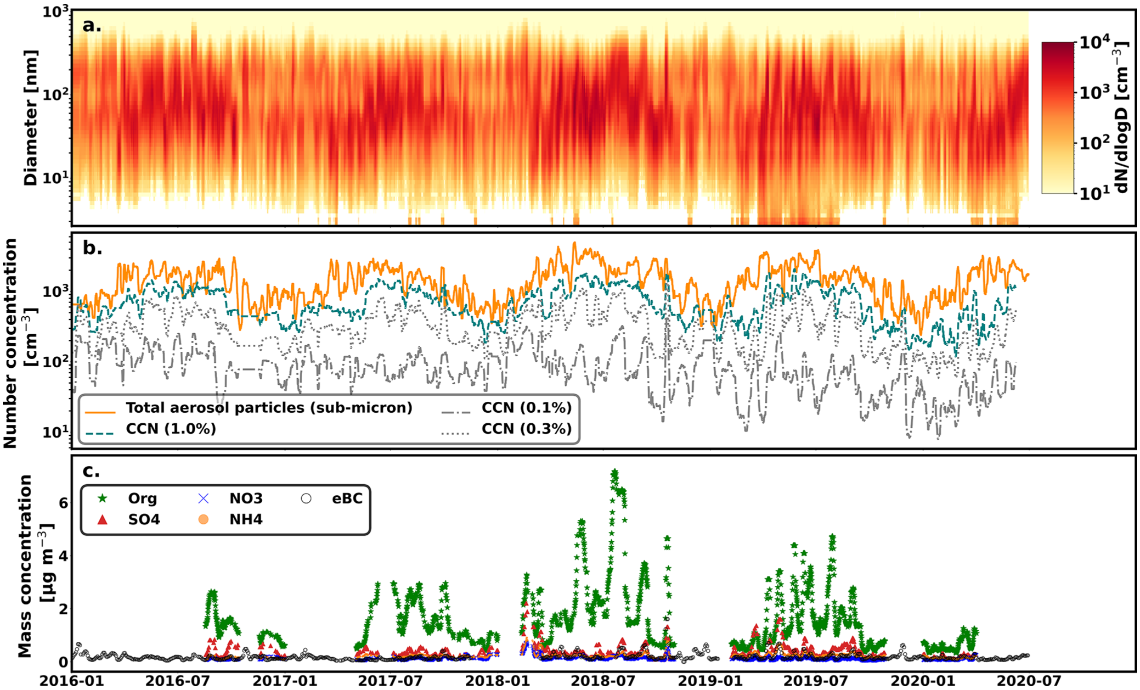

Figure 2. Temporal coverage of the observation data represented through seven-day running median. The top panel **(a)** shows the variation of the aerosol size distribution. The middle panel **(b)** shows the total number concentration of sub-micron aerosol particles (in orange) and CCN at 0.1, 0.3 % and 1.0 % supersaturation (in grey). The bottom panel **(c)** presents the mass concentrations of various chemical species and ions in the aerosol particles: organics (Org), sulfate (SO_4), nitrate (NO_3), ammonium (NH_4), and equivalent black carbon (eBC).

perse mode, where the former is utilized to determine size-segregated N_{CCN}, as detailed in Paramonov et al. (2013). In contrast, the polydisperse mode, employed here, measures the overall N_{CCN} at a given supersaturation.

The CCNc consists of a saturator unit and an Optical Particle Counter (OPC). The saturator is a vertically oriented flow tube, into which aerosol-laden sample air is introduced surrounded by a particle-free sheath air flow (1/10 flow ratio) under laminar flow conditions, forming a well-defined central flow path. The inner walls of the tube are wetted and subjected to a controlled temperature gradient. The sheath air flow is saturated with water vapor at the inlet temperature. A positive temperature gradient is maintained at the saturator column, inducing a quasi-constant supersaturation profile for a specific temperature difference. As the laminar flow progresses through the column, water vapor and heat diffuse from the moist walls toward the center. The effective supersaturation is influenced by factors such as flow rate, pressure, and temperature gradient. While moving through the tube, aerosol particles absorb water and grow and those particles with critical supersaturations lower than the centerline supersaturation are activated as cloud droplets. Droplets larger than 0.75 µm in diameter are detected by the OPC at the exit of the tube and those exceeding 1 µm are considered to be activated CCN. To measure at different supersaturations, the temperature gradient is increased in steps while the flow rate is held constant. Both polydisperse and monodisperse CCN concentrations were measured at each supersaturation setpoint (1.0 %, 0.5 %, 0.3 %, 0.2 %, 0.1 %). At each setpoint, the cycle includes 300 s polydisperse and 600 s monodisperse measurements, with additional stabilisation time after changing supersaturation, yielding a time resolution of about 2 h for this data set. Quantification and discussion of typical uncertainties related to the supersaturation and hence N_{CCN} measured with this instrument are presented in e.g., Rose et al. (2008) and Topping et al. (2005). At SMEAR II, the air to the CCNc is sampled 8 meters above the ground level and features the same inlet as the DMPS (see Sect. 2.1.3.). The aerosol flow rate is 0.5 L min^{-1}, which is split into sheath flow of 0.45 L min^{-1} and sample flow of 0.045 L min^{-1}. For quality assurance of the CCNc data, the CCNc calibration is conducted approximately twice a year using nebulised, dried, charge-equilibrated and size-segregated ammonium sulfate aerosol following procedure as per Rose et al. (2008).

Estimates of smallest activation dry diameter (D_{act}) were derived using the combination of the DMPS and the CCNc data by integrating the PNSDs from their maximum diameters to the diameter at which the integrated particle number was equal to the measured N_{CCN}. D_{act} was then calculated by interpolating between the two adjacent size bins (Furutani et al., 2008). Essentially, variations in activation diameter reflect differences in the chemical composition of aerosol particles: the more hygroscopic the aerosol, the smaller the activation diameter.

2.1.4 Aerosol chemical composition

An Aerosol Chemical Speciation Monitor (ACSM; Ng et al., 2011) was used at SMEAR II to measure the mass concentrations of non-refractory submicron particulate matter ($NR\text{-}PM_1$). The ACSM quantifies ions originating from non-refractory organic and inorganic species and reports them as mass concentrations of sulfate, nitrate, ammonium, and chloride ions, along with total organic aerosol mass. Briefly, the ACSM samples dried ambient air through a critical orifice (100 µm in diameter) with a flow rate of $1.4\,\mathrm{cm^3\,s^{-1}}$ to an aerodynamic lens (Liu et al., 1995a, b), which focuses a submicron particle beam and directs it to the instrument vaporization and ionization chamber. The lens efficiently transmits particles with vacuum aerodynamic diameters (D_{va}) ranging from approximately 75 to 650 nm, yet it also passes through particles up to 1 µm in D_{va} with a less efficient transmission. These aerosol particles then undergo flash vaporization at 600 °C and are subsequently ionized using electron impact ionization (70 eV) and the mass spectrum is obtained with quadrupole mass spectrometry. While the vacuum system of the ACSM efficiently reduces the amount of air molecules entering the instrument detection unit, their distinction from the aerosol components is required. For this purpose, the ACSM contains a 3-way valve system to routinely measure the signals obtained from particle-free air, and this background is subtracted from the particle-laden sample. The detailed description of the ACSM measurements performed at SMEAR II since 2012 is provided in Heikkinen et al. (2020), which includes descriptions of the instrument ionization efficiency calibrations, collection efficiency corrections and data processing. The ACSM measurements were conducted < 100 m away from the DMPS, CCNc and aethalometer measurements in a separate container. A $PM_{2.5}$ cyclone was installed on the container roof, and the ~ 3 m long inlet line had an additional make-up flow of $3\,\mathrm{L\,m^{-1}}$. The air was dried to < 30 % RH with a Nafion dryer. The original time resolution of the ACSM data is ~ 30 min.

We combined the ACSM measurements with measurements of eBC. The eBC concentration was determined based on PM light absorption measured by an aethalometer (Magee Scientific, models AE31 and AE33). For the period in question here (2016–2020), the instrument was changed in the middle as the old instrument broke down. AE31 operated until the end of 2017 and AE33 started measuring in the beginning of 2018. An aethalometer is a filter-based instrument and it measures aerosol light absorption at seven wavelengths (370, 470, 520, 590, 660, 880, and 950 nm). The aethalometer data were corrected for measurement artefacts caused by collecting the particles in a filter medium, the so-called loading effect and scattering caused by the filter material: AE33 applied the inbuilt dual-spot correction (Drinovec et al., 2015) with multiple scattering correction factor 1.39 whereas the AE31 data were corrected as suggested by Virkkula et al., 2007 with multiple scattering correction factor 3.14 (derived by Luoma et al., 2021, for SMEAR II data). The eBC concentration was derived from the absorption at 880 nm channel by using mass absorption cross-section of $7.77\,\mathrm{g\,m^{-2}}$ for AE33 data (the default value suggested by the manufacturer) and $4.8\,\mathrm{g\,m^{-2}}$ for AE31 data (derived from $6.6\,\mathrm{g\,m^{-2}}$ at 637 nm used for multi-angle absorption photometer, which was used as a reference in Luoma et al., 2021). The head of the sampling line was located 4 m above the ground. The concentration of eBC was measured for PM_{10}. Sample air was dried with a Nafion dryer and data was marked as invalid if the relative humidity inside the instrument increased above 40 %. The aethalometer data was converted to STP conditions (273.15 K, 1013.25 hPa).

The published ACSM and eBC measurements data are averaged over 1 h intervals, but to align with the CCN measurements, the data set was further converted to the 2 h time grid by taking a median of the mass concentrations of each of the measured species over the time window of each CCN spectrum measurement. The time series (7 d running median) are shown in Fig. 2c. The data coverage is higher for the eBC data compared to the ACSM data, which has fewer observations during wintertime.

2.1.5 Data coverage and seasonal classification

Figure 2 presents the overall data coverage along with the key aerosol properties observed (see Fig. S2 for the number of data points across different seasons). As mentioned earlier, SOA formation and NPF events lead to higher particle number concentrations during spring and summer. This is also reflected in the variability of CCN, particularly at higher supersaturations (see Fig. 2b), while lower seasonal variation is observed at lower supersaturations ($SS = 0.1$ %), where only larger particles (> 200 nm, see Fig. S3 and Table S1 in the Supplement) are activated. This suggests that most changes in aerosol particle number and chemical composition occur among smaller particles (Aitken and nucleation modes) between the winter and growing seasons (spring and summer). In terms of chemical composition, organics dominate the aerosol mass (see Fig. 2c), especially during the growing seasons, followed by sulfate and ammonium ions, with nitrate and black carbon contributing only minor fractions. However, given the significant seasonal variation in overall aerosol properties at the site, we present the results according to a seasonal classification. In this framework, March, April, and May represent spring; June, July, and August represent summer; September, October, and November correspond to autumn; and December, January, and February correspond to winter.

2.2 Calculations for the forward and inverse closure studies

2.2.1 κ-Köhler theory

The classical Köhler theory (Köhler, 1936) utilizes information about the composition and size of aerosol particles. It estimates the critical supersaturation level SS_{crit} and wet particle diameter at which an aerosol particle becomes activated and grows through condensation to form a cloud droplet. The Köhler equation comprises two terms (see Eq. 1): one accounting for the influence of solutes (the soluble fraction of aerosol particles), which tends to reduce the equilibrium saturation ratio S (defined as $1 + \mathrm{SS}$), and the other known as the Kelvin term, which represents the increased surface tension over a spherical surface. In an aqueous solution, if P (Pa) is the partial vapor pressure of water and P_s (Pa) saturation vapor pressure of water over a pure flat liquid, the equilibrium saturation ratio $S = P/P_s$ is represented as

$$S = a_w \exp\left(\sigma\rho \frac{4M_w}{RT D_{p,wet}}\right) \quad (1)$$

where a_w is the activity of water in the solution, ρ is the density of the solution ($\mathrm{kg\,m^{-3}}$), M_w is the molar mass of water ($0.018\,\mathrm{kg\,mol^{-1}}$), σ ($\mathrm{N\,m^{-1}}$) is the surface tension of the solution, R is the universal gas constant ($8.314\,\mathrm{J\,mol^{-1}\,K^{-1}}$), T is temperature (K), and $D_{p,wet}$ is the diameter of the droplet (m). To facilitate the comparison to previous work, we use the modified version of Köhler theory (Eq. 1) described by Petters and Kreidenweis (2007) to calculate the activation dry diameter (related to the total amount of soluble mass) for a particular supersaturation SS (i.e., $S - 1$, referred to as the κ-Köhler framework

$$S = \frac{D_{p,wet}^3 - D_{p,dry}^3}{D_{p,wet}^3 - D_{p,dry}^3(1-\kappa)} \exp\left(\sigma\rho \frac{4M_w}{RT D_{p,wet}}\right) \quad (2)$$

where $D_{p,dry}$ is the dry diameter of the dry aerosol particle with a given composition described by a unitless hygroscopicity parameter κ. In our calculations, we have assumed that the density and surface tension of the solution are equivalent to those of water ($1000\,\mathrm{kg\,m^{-3}}$ and $0.0728\,\mathrm{N\,m^{-1}}$ respectively). Additionally, we have considered a constant ambient temperature (T) of 298.48 K for all seasons, corresponding to the median temperature inside the measurement hut.

Assuming internally mixed aerosol particles, the net hygroscopicity parameter κ for a mixture of n different chemical species is expressed as the linear combination of the individual species κ_i weighted by their respective volume fractions ε_i in the dry particle (Stokes and Robinson, 1966):

$$\kappa = \sum_i \varepsilon_i \kappa_i . \quad (3)$$

The volume fractions ε_i of the individual components were calculated from the measured mass concentrations, m_i, and their respective densities, ρ_i

$$\varepsilon_i = \frac{\frac{m_i}{\rho_i}}{\sum \frac{m_i}{\rho_i}} \quad (4)$$

Assuming an internally mixed aerosol population is a key assumption made in this study. According to Paramonov et al. (2015), the aerosol in Hyytiälä indeed shows some seasonal and size-dependent mixing state characteristics. Specifically, they report that particles in the ∼ 75–300 nm range are internally mixed during late spring and early summer (May–July), with a very small CCN-inactive fraction (∼ 0.2 %). For the rest of the year, the aerosol becomes partially externally mixed, with the CCN-inactive fraction increasing to ∼ 6.6 %. However, within each size range – either below or above 100 nm – the κ distributions are relatively consistent, suggesting that particles are mostly internally mixed within those size classes.

2.2.2 Forward closure

In the forward closure, N_{CCN} at supersaturations of 0.1 %, 0.2 %, 0.3 %, 0.5 %, and 1.0 % (corresponding to the supersaturations set in the CCNc, henceforth referred to as SS_{CCNc}) are predicted using observations of the aerosol number size distribution from the DMPS. As discussed above, two different assumptions about the hygroscopicity of the aerosol mixture were tested: (1) assuming constant hygroscopicity of 0.18 ($\kappa_{0.18}$) (2) assuming mixture hygroscopicity (Eq. 4) using chemical composition information from the ACSM and aethalometer measurements (κ_{bulk}). κ_{bulk} therefore, does not depend on particle size, but is variable in time. For deriving κ_{bulk} the observed aerosol chemical composition was utilized, assuming that all sulfates are present as ammonium sulfate $(NH_4)_2SO_4$ (AS) and the observed nitrate was distributed between ammonium nitrate NH_4NO_3 (AN) and organic nitrate (ON), estimated using the method explained in Farmer et al. (2010) (see Supplement Sect. S1 and Fig. S4). For the calculation of the AS and AN mass concentration, only the measured sulfate and nitrate mass concentrations were used. The ammonium mass concentration required for yielding ion balance within the particles was calculated (see Fig. S5; Zhang et al., 2007). We acknowledge that the assumption that sulfate is present solely as AS can cause underestimations of aerosol hygroscopicity at SMEAR II (e.g., Riva et al., 2019). Finally, to retrieve the volume fractions of organics, AS, AN, ON and eBC from their estimated mass concentrations, the density information for each species is required. The chosen densities are shown in Table 1 along with the κ_i for each species.

The critical supersaturation SS_{crit} was then calculated for each of the size bins measured by the DMPS using κ-Köhler theory, assuming a uniform composition throughout the size distribution. Particles for which the calculated SS_{crit} was lower than the individual SS_{CCNc} were then considered as

Table 1. Densities (ρ_i) and hygroscopicity parameters (κ_i) of the assumed dry particle constituents based on the composition estimated from the ACSM and the aethalometer measurements.

Species	ρ ($kg\,m^{-3}$)	κ
Organics	1500 (Kostenidou et al., 2007)[a]	0.12 (Pöhlker et al., 2023)
Ammonium nitrate (AN)	1720	0.67 (Petters and Kreidenweis, 2007)
Ammonium sulfate (AS)	1769	0.61 (Petters and Kreidenweis, 2007)
Organic nitrate (ON)	1500[b]	0.12[b]
Equivalent black carbon (eBC)	1770 (Park et al., 2004)	0 (Weingartner et al., 1997)

[a] SOA density estimated to be in the 1400–1650 $kg\,m^{-3}$ range when formed from BVOCs known to produce the majority of SOA at SMEAR II. 1500 $kg\,m^{-3}$ is chosen from this range. [b] Set to equal that of the rest of the organics for simplicity. Some studies suggest that the density could be slightly lower (1160–1210 $kg\,m^{-3}$, Claflin and Ziemann, 2018).

CCN corresponding to the respective SS_{CCNc} value. Linear interpolation was applied to estimate the exact activation diameter within a given size bin (see Lowe et al., 2016). The CCN spectra estimated by the forward closure were then compared to the observations made by the CCNc for the two different hygroscopicity assumptions i.e. κ_{bulk} and $\kappa_{0.18}$.

2.2.3 Inverse closure

In the inverse closure, our objective was to minimize the differences (e.g. through Normalized Root Mean Squared Error, NRMSE, see Sect. 2.2.4) between predicted and observed N_{CCN}, while optimizing the size-dependent chemical composition and hygroscopicity parameter. More specifically, we assumed the size distribution to consist of internally mixed and log-normally spaced Aitken and accumulation modes.

The inverse closure and thus the optimization was performed implementing two different methods, namely the Nelder-Mead and the DREAM-MCMC (DiffeRential Evolution Adaptive Metropolis Markov Chain Monte Carlo) algorithms (see the descriptions of the Nelder–Mead and DREAM-MCMC algorithms). In both optimization methods, all AN and AS masses were combined and treated as inorganic mass for simplicity. The net ρ and κ of the inorganic fraction were derived using the corresponding observed mass fraction. While the κ for AN is slightly higher than that of AS (Table 1) and the density of AN is slightly lower of that of AS (Table 1), we consider this as a reasonable simplification given the low AN concentration at the site. Again, all ON is assumed to have the same κ and ρ as the organics (Table 1). Another key simplification is that eBC is assumed to have the same mass fraction in both modes.

The optimization procedures based on Nelder–Mead and DREAM-MCMC are illustrated in Fig. 3. In both approaches, the derivation of modal optimized hygroscopicity parameters (κ_{opt}^{Aitken} and $\kappa_{opt}^{accumulation}$ from Nelder-Mead method and κ_{MCMC}^{Aitken}, $\kappa_{MCMC}^{accumulation}$ from DREAM-MCMC, referred to as κ_{opt} and κ_{MCMC} for simplicity) begin with obtaining a bimodal fit of the aerosol number size distribution into Aitken and accumulation modes (see Sect. 2.1.2). Next, the fitted lognormal size distribution was binned onto the same diameter axes as the observational data, and the number of particles in each bin was scaled to match the particle number in measured size distribution (see a demonstration in Fig. S6 and Sect. S2). This way, the number contributions of the Aitken and accumulation modes to the observed aerosol size distribution could be estimated for each time point. Second, the masses of the Aitken and accumulation modes were estimated by approximating the density of both modes by the bulk density. The total masses of organics, inorganics and eBC to be distributed to the measured size distribution were then calculated using the mass fractions derived from the ACSM and aethalometer measurement. Finally, the Aitken vs. accumulation mode compositions, and hence κ_{opt} or κ_{MCMC}, were determined through optimization (see also Sect. S3 for details).

Nelder-Mead

The Nelder–Mead simplex algorithm (Gao and Han, 2012) is suitable for both one-dimensional and multidimensional optimization problems and is relatively fast in our application. In our case, we need to optimize only one variable (the fraction of total organic mass in Aitken mode, $m_{org,Ait}$) and the remaining masses can be derived from it through mass closure constraints – assuming PNSD to stay constant throughout each CCN measurement cycle. For each time step, the optimization begins with an initial simplex of three trial values of $m_{org,Ait}$, and the NRMSE is evaluated at each point. The worst-performing value is reflected across the midpoint of the better two to explore whether a more accurate estimate can be found in the opposite direction. If this improves the fit, the algorithm attempts an expansion, pushing further in the same direction. If reflection does not improve the result, a contraction step is taken to move closer to the midpoint. If neither reflection nor contraction improves the outcome, the simplex undergoes shrinkage, tightening around the best-performing solution to focus the search locally. This process continues until the optimization converges, resulting in an estimate of $m_{org,Ait}$ that minimizes the NRMSE between modeled and observed CCN concentrations. Note that Nelder–Mead works well for simple, low-dimensional problems like

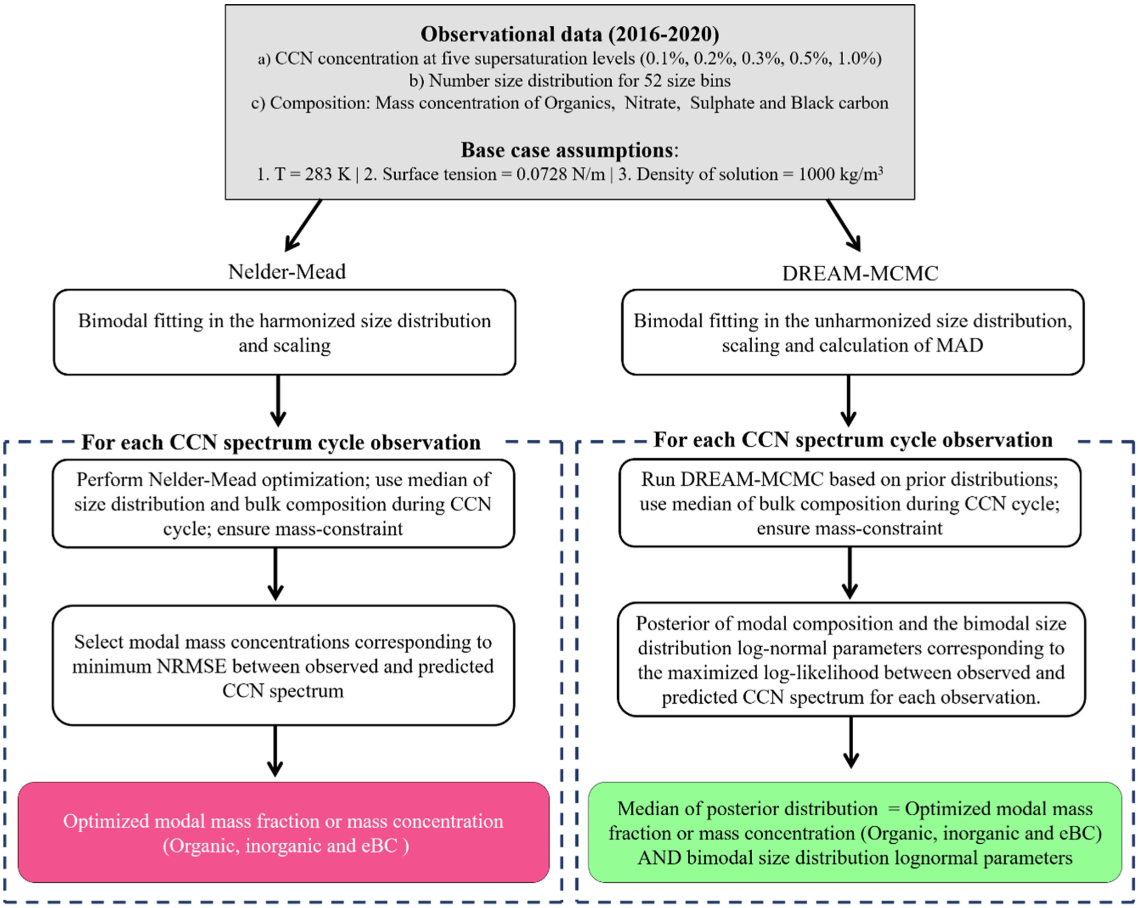

Figure 3. Workflow of the two inverse closure methods: the Nelder–Mead algorithm (left) and the DREAM-MCMC (right) approach. Bimodal fitting: representation of the aerosol size distribution as two lognormal modes. Harmonized size distribution: size distribution data harmonized to CCN data; data thus obtained has 2 h resolution. Unharmonized size distribution: raw size distribution data with 10 min resolution. Scaling: adjustment of number concentrations of reconstructed lognormal size distribution from bimodal parameters to match observations. Mass-constraint: conservation of total aerosol mass (sum of mass in two modes) of each species during optimization. NRMSE: normalized root mean square error, a metric of model–observation agreement. MAD: median absolute deviation, used to quantify variability in size distributions during CCN spectrum cycle period. Prior distribution: initial parameter ranges provided to the MCMC sampler. Log-likelihood: statistical measure of consistency between observed and modeled CCN spectra.

optimizing just one parameter (e.g., $m_{\mathrm{org,Ait}}$), but it starts to struggle as the number of variables increases and have a tendency for converging to local minima.

DREAM-MCMC

In order to assess the importance of the variability of the bimodal size distribution parameters within each CCN cycle, we conducted a second inverse-closure experiment with the number concentration and mean diameter for both modes as additional optimization parameters (simultaneously with $m_{\mathrm{org,Ait}}$). Since optimizing both size distribution parameters and composition introduces a more complex and higher-dimensional parameter space, and we are interested parameter uncertainty, we use a Bayesian inference approach to estimate the parameter posterior distributions. Specifically, we chose the DiffeRential Evolution Adaptive Metropolis Markov Chain Monte Carlo (DREAM-MCMC) algorithm (Vrugt et al., 2009), which has been previously used for inverse CCN-closure studies in idealized cases (Partridge et al., 2012) and is available in the Python PINTS library (Clerx et al., 2019). DREAM-MCMC is an efficient MCMC method (Metropolis et al., 1953; Gelfand and Smith, 1990) that evaluates multiple Markov chains in parallel and automatically adapts its proposal strategy during sampling, making it particularly efficient for correlated, multi-modal problems such as aerosol-cloud microphysical interactions. To know more about MCMC and Bayesian inference, see Sect. S4.

We initialized the MCMC optimization with Cauchy priors for each parameter (see Sect. 5), centered on the median values of the fitted bimodal size distributions for each CCN cycle, specifically, the number concentration and GMD. For chemical composition we used the median of the ACSM observations during each CCN spectrum cycle. The scale value was the smaller of either 1 (resulting in a Student-t distribution) or the median absolute deviation (MAD) of the observations within the given CCN cycle. The priors were truncated to positive values only. We also constrained the total aerosol mass in each mode to remain within ±10 % of the total mass observed by the ACSM and aethalometer.

We used a heteroskedastic Gaussian likelihood function, which means that the highest likelihood is typically where the parameters provide the least squares fit to the CCN observations, analogous to minimizing the NRMSE described above. The likelihood is defined as

$$L(\theta|Y) = \prod_{i=1}^{n} \frac{1}{\sqrt{2\pi s_i^2}} \exp\left[-\frac{1}{2} s_i^{-2} (y_i - \phi_i(\theta))^2\right] \tag{5}$$

where s_i is standard deviation of the measurement error, which we assume is 10 % of the CCN observations at each supersaturation value y_i and ϕ_i is the model predictions of CCN spectra at each super-saturation given the calibration parameters θ (the log-normal parameters and mass fraction). We performed the optimization in a log-transformed parameter space, which improves sampler efficiency by normalizing scale differences between parameters. For each CCN observation window, we ran five chains with 40 000 iterations per chain, of which the first 15 000 were used as burn-in/adaptation. Up to two chains were discarded if they deviated strongly in central tendency after burn-in, and the last 20 000 steps of all accepted chains were then used to calculate posterior statistics. Convergence was assessed with the $\hat{R}$-statistic (Gelman and Rubin, 1992), using a relaxed threshold of $\hat{R} < 2.5$ for all five parameters to retain a window in the analysis. The $\hat{R}$-statistic compares the variance within chains to the variance between chains; values close to 1 indicating well-mixed, converged chains. We used a relaxed threshold because the $\hat{R}$-statistic is quite conservative and because our problem has high correlation between parameters and the potential for multi-modality if there are multiple distinction aerosol populations within one window, which is penalized by the $\hat{R}$-statistic but realistic in this case. Overall, 19 % of windows were discarded due to high $\hat{R}$-statistic values. Even with the relaxed threshold, some windows were excluded where the MCMC identified reasonable parameter values and CCN spectra but the chains failed to mix well. Examples of the chain evolution and posterior parameter distributions are discussed in Sect. S5.

2.2.4 Metrics for assessing variability of lognormal size distribution parameters during CCN cycle

Unlike the Nelder–Mead optimization method, which uses the median of the size distribution during the CCN cycle period, the DREAM-MCMC setup requires the variability of the size distribution as input. To account for this, we calculate the median absolute deviation (MAD) of each lognormal parameter for every CCN cycle observation. The overall distribution of MAD values for the full 5-year dataset is presented in Sect. S6 and Fig. S10. MAD for individual CCN cycle period is calculated as follows:

Let $I_c = [t_c^{\text{start}},\ t_c^{\text{end}})$ be the time window for CCN cycle c; For a given lognormal parameter, k(among geometric mean diameter (GMD), geometric standard deviation (SD) and number concentration in each mode; so total 6 parameters), collect the samples inside this window as $\{x_k(t) : t \in I_c\} = \{x_{k,1}, x_{k,2}, \ldots, x_{k,\,n_c}\}$.

Median in the interval is $m_k(c)$:

$$\text{median}\{x_{k,1}, x_{k,2}, \ldots, x_{k,n_c}\} \tag{6}$$

MAD in interval c:

$$\text{median}|x_{k,i} - m_k(c)|, \text{ where } i \text{ varies from 1 to } n_c \tag{7}$$

2.2.5 Metrics for assessing the goodness of closure

The Normalized Root Mean Square Error (NRMSE) between observed and predicted CCN concentrations was calculated as (see also Sect. S7 and Fig. S11):

$$\text{NRMSE} = \frac{\sqrt{\frac{1}{n}\sum_{i=1}^{n}\left(\text{CCN}_{\text{pred},i} - \text{CCN}_{\text{obs},i}\right)^2}}{\overline{\text{CCN}_{\text{obs}}}} \tag{8}$$

where $\text{CCN}_{\text{pred},i}$ is the predicted CCN concentration at supersaturation i, $\text{CCN}_{\text{obs},i}$ is the observed CCN concentration at supersaturation i, n is the number of data points (in this case five, as we have five different supersaturations) and $\overline{\text{CCN}_{\text{obs}}}$ is the mean of the observed CCN concentrations across all supersaturations.

To facilitate direct comparison with Schmale et al. (2018) we also calculated the Geometric Mean Bias (GMB) for each time point, defined as:

$$\text{GMB} = \exp\left(\frac{1}{n}\sum\nolimits_{i=1}^{n} \ln\left(\frac{\text{CCN}_{\text{pred},i}}{\text{CCN}_{\text{obs},i}}\right)\right) \tag{9}$$

3 Results and discussion

3.1 Size distributions and activation diameters

Figure 4 presents the median and quartiles of lognormal aerosol number size distributions and median activation diameters (D_{act}) calculated from the PNSD-CCN closure across different seasons. In PNSD–CCN closure, D_{act} at a given SS was derived by integrating the PNSD from the largest to the smallest diameters until the integrated number equalled the measured CCN concentration at that SS; the corresponding diameter was then identified as D_{act} (see e.g. Sihto et al., 2011 and Sect. S8). The shape of a lognormal size distribution depends on the age of the aerosol population, and the atmospheric processing (e.g. nucleation, coagulation, condensation, deposition and chemical reactions) that has taken place along the transport trajectory to the measurement site. As discussed previously, NPF (Nieminen et al., 2014) and biogenic SOA formation (Heikkinen et al., 2020) result in almost bell-shaped size distributions with high particle number concentrations in spring and summer. In autumn and winter, on the other hand, biogenic aerosol precursor emissions are reduced leading to a lowering in the organic aerosol mass fraction. The contribution from long-range transported, cloud-processed and aged particles increases, detected in the form of bimodal aerosol size distributions with predominant Hoppel minima (Hoppel et al., 1986) at around 80–90 nm in diameter, and increased inorganic aerosol mass fractions. The activation diameters decrease with increasing supersaturation and the median D_{act} (see Table S1) is generally higher for all seasons than reported in earlier studies using similar methodology (e.g., Sihto et al., 2011; Paramonov et al., 2015). For instance, Paramonov et al. (2015) reported a median D_{act} of 46 nm at 1.0 %, whereas we find values of 54–57 nm. Similarly, at 0.1 % supersaturation, they reported 150 nm, which is lower than our results of 206–224 nm, depending on the season. This could reflect decreasing abundance of sulfate during the last two decades as compared with less hygroscopic organic species (Fig. S12; see also Aas et al., 2019; Li et al., 2024). The activation diameters are relatively similar across the seasons (see Table S1), therefore suggesting a similar composition of the CCN over the year in comparison with the variability in the number size distribution. The slope of the PNSD function is typically steep over the ranges of D_{act} corresponding to the investigated supersaturations. This indicates a high sensitivity of CCN to any parameters driving the PNSDs (see e.g., Lowe et al., 2016). While the median activation diameters show almost no seasonality, looking in more detail (see Fig. S3), an increase in the D_{act} is observed during the transition from winter to spring. This is probably due to the addition of more organic aerosol, which is less hygroscopic than the common inorganic salts. D_{act} reaches its maximum in summer and decreases again towards autumn. After autumn, there is an increase in D_{act} toward winter, despite a decrease in BVOC emissions and the resulting lower organic mass fraction alongside a higher inorganic fraction (see Fig. S13). This suggests the influence of another factor, possibly the higher eBC fraction observed during winter (see Sect. 3.3).

While the seasonal variation in median activation diameters D_{act} is not pronounced across all SS, more detailed inspection (Fig. S3) reveals a decrease in D_{act} at the lowest supersaturation (0.1 %) during the transition from autumn into winter (November to April). This trend is consistent with a reduced contribution of organic aerosols and a higher relative abundance of inorganic components during winter (sources of which include long-range transport and e.g. cloud-processing along the transport route), as also indicated by the bulk chemical composition (Fig. S13). Since the activation diameters at 0.1 % SS fall within the accumulation mode, the size range where ACSM measurements are most representative, the observed seasonal variation in D_{act} at this SS level can be directly linked to changes in aerosol composition. Overall, across all supersaturations, an increase in D_{act} is generally observed during the transition from spring to summer which is more pronounced at 0.1 %, 0.2 %, and 1.0 % SS, while being relatively weak at 0.5 % SS.

3.2 CCN spectra – Insights from forward and inverse CCN closures

Figure 5 shows the comparison between the observed and predicted CCN spectra, again displayed for each season separately. First, seasonal variations are evident, with CCN concentrations peaking in the summer and having their minimum in winter – in line with the overall particle number concentrations (see Figs. 4 and S14). The median seasonal CCN concentration ranges from 29–76 $\mathrm{cm^{-3}}$ for 0.1 % supersaturation, 101–317 $\mathrm{cm^{-3}}$ for 0.2 %, 143-512 $\mathrm{cm^{-3}}$ for 0.3 %, 170-744 $\mathrm{cm^{-3}}$ for 0.5 %, and 300–1116 $\mathrm{cm^{-3}}$ for 1.0 % with significant variations across seasons. These values are somewhat lower than previous studies (Sihto et al., 2011; Paramonov et al., 2015), potentially related to decreases in overall particle number concentrations and a more prominent role of biogenic organic aerosols vs. inorganic sulfate (see e.g., Li et al., 2024) – reflecting the higher activation diameters reported here as compared to the previous studies. The NRMSE values for the two forward closure methods range from 0.42 to 0.94 (Table 2). The agreement of the forward closure based on the bulk composition is best for supersaturations of 0.2 % and 0.3 % where the activation diameter is generally within the accumulation mode range, and hence also the ACSM composition is probably a more accurate estimate of the composition of the dry particles. The agreement is worst for the lowest supersaturation of 0.1 %, as also observed previously in Wang et al. (2010) and Meng et al. (2014). Furthermore, the agreement is better during spring and summer compared to autumn and winter (Fig. 5). Interestingly, when comparing the results from the forward closures, a better closure is obtained with the simple constant value of $\kappa_{0.18}$ than with the "bottom-up" hygroscopicity estimate using the ACSM and aethalometer data (κ_{bulk}), indicating that assuming size-independent but temporally varying composition performs worse than a much simpler assumption. The results from the inverse closure (κ_{opt}) however, show that this issue can be mitigated when distributing the measured/estimated inorganic and organic species between the Aitken and accumulation modes. Including the size-dependent chemical composition, the variability of the size distribution during CCN cycles and uncertainty in CCN measurements (10 %; see e.g. Rejano et al., 2024 and references therein) further reduces the bias, correcting most of the overprediction (see Fig. 5, κ_{MCMC}). All methods (both the

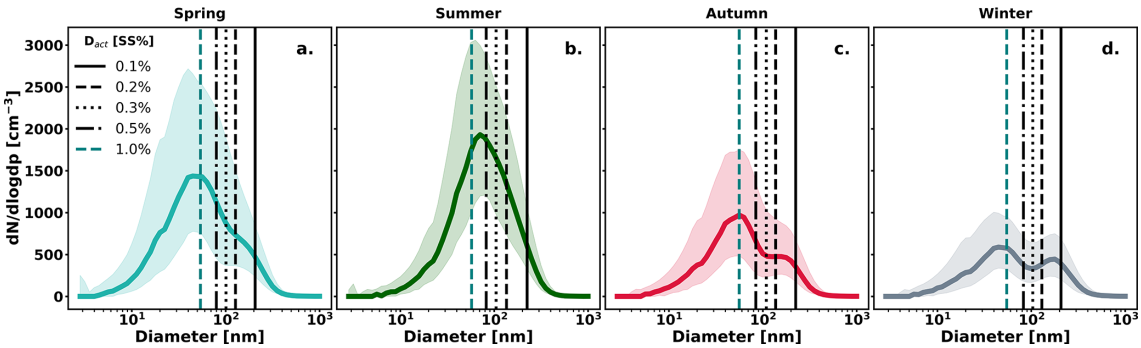

Figure 4. Seasonal overview of the lognormal size distribution, with solid lines representing the median and shaded regions indicating the interquartile range. The vertical lines denote the activation diameters (D_{act}) at various supersaturations as determined by combining the CCN data with the number size distribution measurements from the DMPS.

forward and inverse closures) tend to overpredict CCN numbers, with κ_{bulk} exhibiting the highest error, which is clearer when we look at NRMSE and GMB values (Fig. 6, Table S2 and Fig. S15).

When combined across all SS the overall NRMSE values for the entire timeseries are 0.43 for κ_{bulk}, 0.35 for $\kappa_{0.18}$, 0.28 for κ_{opt} and 0.08 for κ_{MCMC}. To provide a more detailed perspective, we also calculated the NRMSE for each SS individually. Figure 6 provides an overview of how the four different methods perform in estimating CCN concentrations. All methods demonstrate a strong positive correlation with the observations (Pearson $R > 0.70$) and the NRSME remains in most cases below 1.0 (Table 2 and Fig. 6). The performance skill (i.e., the combined behavior of R and NRMSE; see Fig. 6) varies with SS, but when averaged across all SS, κ_{MCMC} achieves the best agreement, followed by κ_{opt}, $\kappa_{0.18}$ and κ_{bulk}. As shown in Table 2, the largest errors generally occur at the lowest (0.1 %) and highest (1.0 %) supersaturations. An exception is κ_{MCMC}, which substantially reduces the bias and NRMSE across all supersaturations. The highest error is still at 0.1 %, while the other supersaturations agree closely with the observations. At 0.5 % SS, the NRMSE for κ_{bulk} is around 0.56 and the GMB is around 1.38 (see Fig. S15 and Table S2), which is slightly higher than the GMB (1.32) reported by Schmale et al. (2018) for a shorter dataset and a different time period. The best performance skill for the forward closure is obtained at SS = 0.3 %, followed closely by SS = 0.2 % (see Table 2), where predominantly accumulation mode particles activate (see Fig. 4). Given that the typical $\mathrm{SS}_{\mathrm{max}}$ in stratocumulus clouds in the region are often below 1 % (Roberts et al., 2006; Hegg et al., 2009), the performance at these levels is particularly relevant. The different SS-dependence of the bias in the MCMC inverse closure as compared with the other closure methods suggests that the source of the bias for the lowest supersaturation differs from that at higher supersaturations. For the lowest supersaturations, the high flow rate in the CCN counter may hinder smaller particles from growing sufficiently to be detected by the CPC (see also Ervens et al., 2007; Lance et al., 2006). For the highest supersaturation, our results suggest that the significant over-prediction of the forward-closure and Nelder-Mead methods are indeed a result of the high variability of the PNSD and the sensitivity of the Aitken-mode CCN to it.

The results presented in Fig. 5 reveal a systematic overprediction of N_{CCN}. Part of this overprediction could be remedied by assuming a size-dependent chemical composition with an enrichment of organics in the Aitken mode – given the expected lower κ of the organic as compared with the inorganic aerosol components. Previous studies have observed that the κ of OA can be even lower than the assumed value of 0.1 (see e.g., Rastak et al., 2017; Cai et al., 2018 and references therein). An alternative way to optimize the results could therefore be through assuming a size-independent composition but lower organic κ. As a conservative evaluation of this approach, we conducted a test assuming organics to be non-hygroscopic, similar to black carbon. In Table 2 and Fig. 6 these calculations are denoted with $\kappa_{\mathrm{org}} = 0$. The resulting NRMSE and GMB (see also Figs. S15, S16 and Sect. 9) suggests that organics in the accumulation mode are likely hygroscopic, as assuming zero hygroscopicity leads to underprediction of N_{CCN}. Another explanation could be due to an under-representation of larger inorganic particles in the observations, for example in the upper tail of the accumulation mode, or an undetected coarse mode component such as sea salt which is not measured by the ACSM. Alternatively, the finding may arise from the initial assumption of the equal distribution of BC among Aitken and accumulation modes. In terms of correlation, κ_{opt}, in comparison to $\kappa_{\mathrm{org}=0}$, consistently performs better overall (see Table 2), the NRMSE values also being smaller than for the entirely non-hygroscopic organics. This suggests that, compared to the variation in the hygroscopicity parameter of organics with size, accounting for the size-segregated nature of chemical composition provides a more accurate explanation for the overprediction of CCN than simply non-hygroscopic organics. The impact of

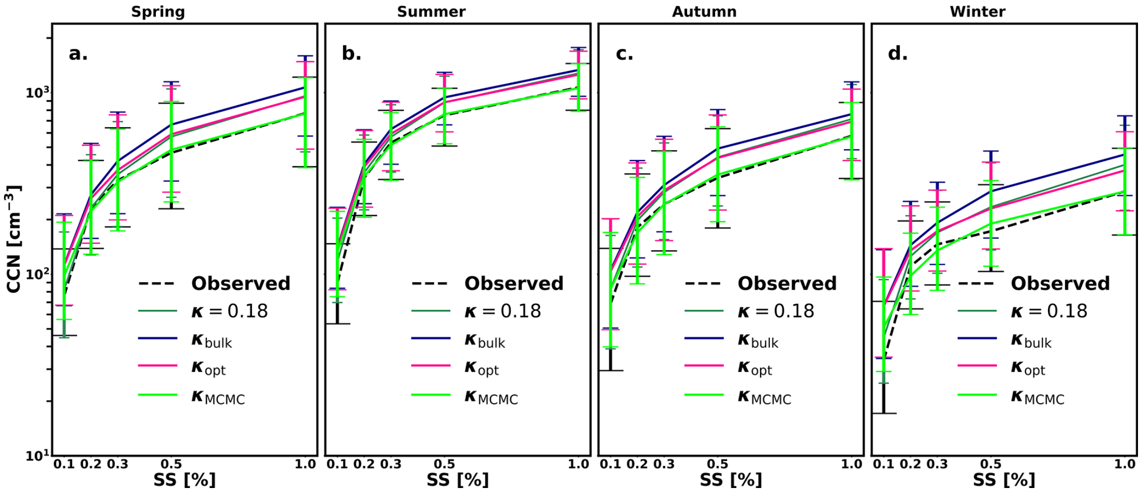

Figure 5. Observed (dashed) and predicted (solid) median CCN spectra in different seasons. The whiskers display the 25th and 75th percentiles.

Table 2. NRMSEs and Pearson's correlation coefficient (R in brackets) corresponding to different methods and supersaturations for all years taken together.

Methods	NRMSE (R) SS = 0.1 %	NRMSE (R) SS = 0.2 %	NRMSE (R) SS = 0.3 %	NRMSE (R) SS = 0.5 %	NRMSE (R) SS = 1.0 %
κ_{bulk}	0.94 (0.78)	0.49 (0.85)	0.49 (0.85)	0.59 (0.84)	0.60 (0.79)
$\kappa_{0.18}$	0.71 (0.74)	0.43 (0.84)	0.42 (0.86)	0.50 (0.85)	0.52 (0.81)
κ_{opt}	0.92 (0.78)	0.46 (0.86)	0.43 (0.87)	0.47 (0.88)	0.44 (0.86)
$\kappa_{org} = 0$	0.62 (0.70)	0.49 (0.75)	0.48 (0.77)	0.46 (0.80)	0.47 (0.77)
κ_{MCMC}	0.65 (0.85)	0.17 (0.97)	0.12 (0.99)	0.082 (0.99)	0.045 (0.99)

assuming constant BC fraction in both modes was also found to be minor (see Sect. S10). Using the DREAM-MCMC optimization to account for the variability of the PNSD during the CCN measurement cycle mitigates most of the overpredictions – further strengthening the strong role of size-dependent chemical composition as key factor for yielding a successful CCN closure, but also highlighting the importance of the PNSD variability.

3.3 Insights on size-dependent submicron hygroscopicity parameter and aerosol composition from inverse CCN closure

For the optimized CCN spectra (κ_{opt} and κ_{MCMC}), the seasonal probability distributions of the corresponding hygroscopicity parameters for Aitken and accumulation modes are shown in Fig. 7. Both optimization approaches produce almost identical κ distributions for the accumulation mode with median hygroscopicity values around 0.2–0.3. In contrast, the Aitken mode exhibits a distinct bimodality in both cases. The Nelder–Mead optimization produces a sharp peak at $\kappa_{Aitken} \approx 0.1$, whereas the DREAM–MCMC distribution shows a lower but broader peak slightly above 0.1 – which would be in line with the expected hygroscopicities of the BVOC oxidation products present at the measurement site. A secondary peak generally appears between $\kappa_{Aitken} = 0.5$ and 0.6, with κ_{MCMC} consistently shifted toward the lower end of this range. The exception is winter, where the second peak is more diffuse in both methods. The lower peak in DREAM–MCMC compared to Nelder–Mead reflects differences in how the two methods balance CCN overprediction. Since κ_{bulk} systematically overestimates CCN, the Nelder–Mead optimization compensates by assigning the Aitken mode a much lower hygroscopicity (higher organic fraction). When size-distribution parameters are also allowed to vary, as in κ_{MCMC}, part of this CCN overprediction can instead be explained by variability in size distribution lognormal parameters. Consequently, the smaller κ peak is reduced in height, while the overall distribution remains consistent with the Nelder–Mead method. In general, the probability distribution of Aitken and accumulation mode hygroscopicity parameter from both methods indicates that the Aitken mode can be predominantly organic on a significant number of instances, with most values of κ clustering around typical organic κ of 0.1. This significant difference in hygroscopicity between the two modes exceeds the typical variability in hygroscopicity values observed for various soluble chemical compo-

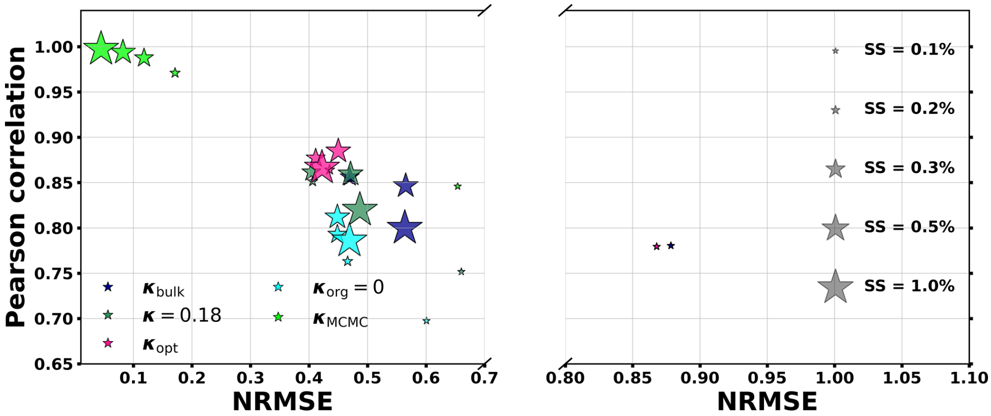

Figure 6. Normalized Root Mean Square Error (NRMSE) and Pearson correlation for different supersaturation (SS) levels for all years taken together, comparing four methodologies: κ_{bulk}, $\kappa_{0.18}$, and κ_{opt}, $\kappa_{org} = 0$ and κ_{MCMC}. The two panels split the NRMSE axis to highlight the data in separate ranges, with the left panel covering NRMSE values from 0.01 to 0.7 and the right panel from 0.8 to 1.1. Each point is sized according to the corresponding SS level (0.1 %, 0.2 %, 0.3 %, 0.5 %, and 1.0 %). The markers are color-coded based on the method for calculating the hygroscopicity parameter, with lines added to represent a discontinuity in the x-axis.

nents, suggesting indeed distinct chemical compositions and water uptake properties of the two modes. Overall, in κ_{opt}, the variability between seasons is similar for both the Aitken and accumulation mode (see Fig. S17), while in κ_{MCMC} the Aitken mode has a significantly higher variability in all seasons. In autumn and winter, the MCMC distributions resemble those from the Nelder-Mead, suggesting a clear organic enrichment in the Aitken mode as compared with the accumulation mode. For the spring and summer however, the distributions of Aitken mode hygroscopicities are more bimodal. The cases where a clear organic enrichment in the Aitken mode is predicted are characterized by relatively high Aitken mode particle number concentrations and large modal diameter. These results are generally in line with previous studies reporting differences in the hygroscopicity of Aitken and accumulation mode-sized particles (Hämeri et al., 2001; Paramonov et al., 2015). Because the Aitken mode hygroscopicity distributions are bimodal, a single central metric (e.g., the median) can under-represent the distribution. Even so, both approaches reveal some common seasonal patterns: Aitken κ is higher in spring and summer, and lower in autumn and winter. In the darker seasons, reduced/absent NPF events and weaker local aerosol production make the accumulation mode more frequently the more hygroscopic mode, while in spring–summer Aitken κ more often approaches or exceeds accumulation values. Accumulation-mode κ remains comparatively stable, typically between 0.2–0.3, with the highest values in winter. This seasonal variability coincides with enhanced summertime photochemistry, which drives new Aitken particle formation from organic vapors and subsequent aging that increases the oxygen-to-carbon ratio of organics, thereby raising their hygroscopicity (Jimenez et al., 2009; Heikkinen et al., 2021).

Because a bimodal distribution in κ was observed with the MCMC optimization, we separated the optimized data into two groups: cases where $\kappa_{Aitken} > \kappa_{accumulation}$ and cases where $\kappa_{Aitken} < \kappa_{accumulation}$. The mean optimized compositions for these groups are shown in Fig. 8, while the corresponding medians are given in Tables S4–S7. In the Nelder–Mead optimization, $\kappa_{Aitken} > \kappa_{accumulation}$ occurs in 23 % of cases, compared to 54 % with the MCMC method. Conversely, $\kappa_{Aitken} < \kappa_{accumulation}$ is found in 77 % of cases with Nelder–Mead and 46 % with MCMC (see Table S8). Despite these differences in frequency, the median κ values shows remarkable agreement between the two approaches (see Table S8). For $\kappa_{Aitken} > \kappa_{accumulation}$, the median GMD_{Aitken}, $GMD_{accumulation}$, κ_{Aitken}, and $\kappa_{accumulation}$ are 30–32 nm, 133–137 nm, 0.5, and 0.2, respectively. In contrast, for $\kappa_{Aitken} < \kappa_{accumulation}$, they are 37–43 nm, 137–164 nm, 0.1, and 0.27. Thus, cases with higher Aitken κ are characterized by smaller Aitken GMD and occurred throughout the year but were much more frequent in summer. This feature has also been reported in previous studies from various environments, where κ increased at diameters typical of Aitken and nucleation mode (particularly below 60–70 nm) and was often – but not always – associated with NPF events (Lance et al., 2013; Spitieri et al., 2023; Massling et al., 2023). For $\kappa_{Aitken} > \kappa_{accumulation}$, the Aitken mass is consistently lower than in the $\kappa_{Aitken} < \kappa_{accumulation}$ case (see Fig. 8), reflecting the availability with condensable vapors with low enough volatility to overcome the Kelvin barrier and condense on the Aitken mode. In both optimization methods, the composition patterns within each group are very similar, just as with the κ values (Fig. 8). For cases where $\kappa_{Aitken} > \kappa_{accumulation}$, the Nelder–Mead predicted the Aitken mode to be almost entirely inorganic, while DREAM-MCMC suggested slightly more organic material but still

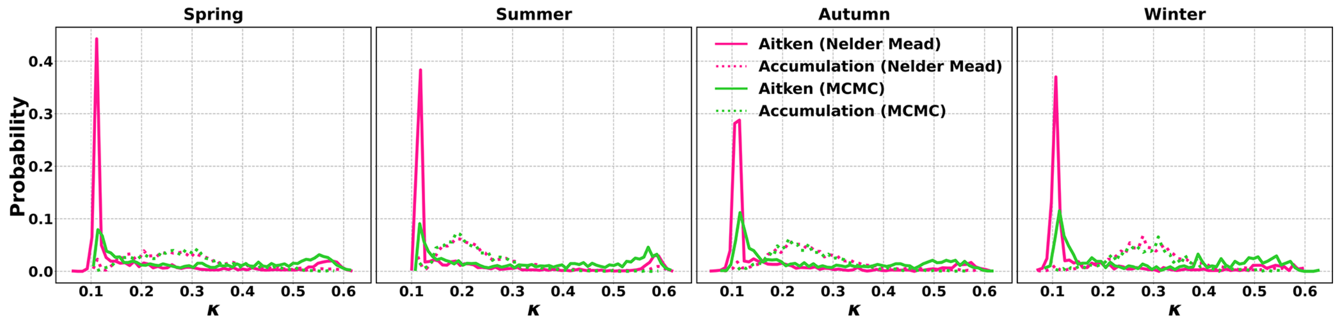

Figure 7. Seasonal probability distributions of the hygroscopicity parameter (κ) for the Aitken and accumulation modes. Each panel corresponds to one season: spring, summer, autumn, and winter. Distributions are shown separately (see legends) for Nelder–Mead optimization and DREAM-MCMC.

mostly inorganics. In these cases, both approaches agree that the Aitken mode had the lowest organic fraction in winter and spring. For $\kappa_{\mathrm{Aitken}} < \kappa_{\mathrm{accumulation}}$, our results, consistent with previous studies at SMEAR II (e.g., Allan et al., 2006), indicate that the accumulation mode contained a larger inorganic fraction, leading to higher hygroscopicity compared to the Aitken mode. Such a difference has also been observed in other similar environments (Timonen et al., 2008; Hao et al., 2013; Levin et al., 2014) as well as in urban Beijing (see also Wu et al., 2016). This disparity in mass fractions of inorganics between the two modes is most pronounced in winter (for example in Nelder-Mead optimization, the relative enrichment in Aitken vs. Accumulation model mass fraction being $\sim 156\,\%$) and autumn (the relative enrichment of $\sim 106\,\%$), i.e. the periods when the distinction between Aitken and accumulation modes is most evident (see Fig. 4). This seasonal variation reflects shifts in aerosol sources and processes, and the results are generally in line with what is known. During summer, biogenic SOA is a major source of particulate matter in Hyytiälä (Heikkinen et al., 2021; Yli-Juuti et al., 2021). In contrast, autumn and winter are characterized by a higher mass fraction (and concentration) of inorganic aerosol chemical components (Heikkinen et al., 2020), which highlights the prevalence of transported (Riuttanen et al. 2013) and cloud-processed particles (Isokääntä et al., 2022). Cloud processing leads to both the observed bimodal PNSD (Fig. 3) and a higher sulfate abundance in the accumulation mode (e.g., Leaitch et al., 1996; Roelofs et al., 1998; Kreidenweis et al., 2003; Wonaschuetz et al., 2012; Ervens et al., 2018).

In our analysis, we assumed values of organic properties (κ and density) based on past studies, as mentioned in Table 1. However, to discard any possibility of major changes in the results, we performed additional inverse-closure studies allowing organic properties to vary in several ways, as discussed in Sect. S11. These sensitivity tests showed that two of the optimization approaches led to physically unrealistic organic densities (~ 1000 and $> 2500\,\mathrm{kg\,m^{-3}}$), despite achieving similar NRMSEs. In contrast, the method keeping the size distribution to the median values observed during CCN cycles produced physically reasonable ρ_{org} (~ 1200–$1300\,\mathrm{kg\,m^{-3}}$) and κ_{org} (0.06–0.08), consistent across seasons – also in the light of typical hygroscopicity values of organic molecules such as those resulting from BVOC oxidation (e.g. Petters and Kreidenweis, 2007; Siegel et al., 2022). This confirms that the assumed organic properties used in the main analysis are robust and do not significantly bias the optimized results.

4 Conclusions

In this study, we integrated long-term chemical composition measurements from an Aerosol Chemical Speciation Monitor (ACSM) with Cloud Condensation Nuclei (CCN) observations and aerosol number size distributions. This resulted in ~ 6200 concurrent two-hour resolution data points. We used this dataset to evaluate four methods for predicting CCN concentrations based on κ-Köhler theory across varying supersaturations, beginning with two forward closure approaches. The first, a 'bottom-up' method, used ACSM and aethalometer data to estimate the bulk hygroscopicity parameter (κ_{bulk}) for predicting CCN concentrations, while the second approach ($\kappa_{0.18}$) assumed a constant κ value of 0.18, as recommended by Sihto et al. (2011), throughout the study period. We observed that the overall median activation dry diameters (D_{act}) ranged from 54 nm ($\mathrm{SS} = 1\,\%$) to 224 nm ($\mathrm{SS} = 0.1\,\%$) nm across different months, suggesting that Aitken mode particles contribute to the CCN numbers at this location – besides the well-known contribution of the accumulation mode (Pierce et al., 2012 and references therein). Therefore, the possibility of different chemical composition/hygroscopicity between Aitken and accumulation modes (for e.g. Broekhuizen et al., 2006) motivated us to use an inverse closure technique that involved an optimization algorithm (Nelder-Mead in the Python SciPy library and DREAM-MCMC) to determine the optimal modal hygroscopicity (κ_{opt} and κ_{MCMC}) by obtaining a closure between observed and predicted CCN concentrations.

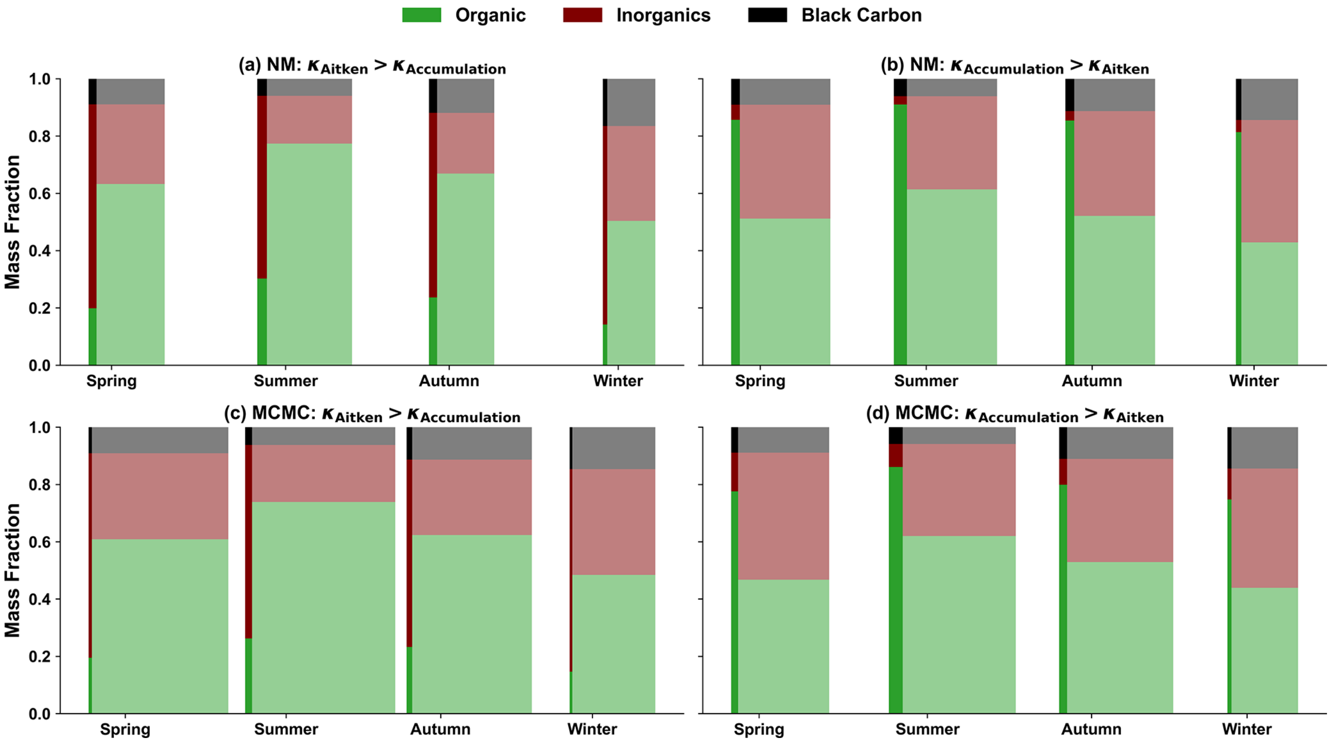

Figure 8. Seasonal mean mass fractions of organic, inorganic, and black carbon components in Aitken and Accumulation modes from Nelder-mead (NM) and DREAM-MCMC optimizations. Panels show cases where $\kappa_{\mathrm{Aitken}} > \kappa_{\mathrm{accumulation}}$ (**a**: NM, **c:** MCMC) and $\kappa_{\mathrm{Aitken}} < \kappa_{\mathrm{accumulation}}$, (**b**: NM, **d**: MCMC). The stacked bars represent the contributions of organic (green), ammonium sulfate (maroon), and black carbon (black) components within each mode. Aitken mode is depicted with solid colors, while Accumulation mode is represented with slightly faded colors. The width of the bars has been scaled to the mass concentration in the corresponding mode.

CCN concentrations at Hyytiälä exhibit clear seasonal variations, peaking in summer and reaching their lowest in winter, reflecting overall particle number trends. Our closure calculations agree reasonably well with observed CCN concentrations, with Pearson correlations exceeding 0.8. However, all of the applied methods tend to overpredict CCN concentrations to varying degrees. As expected, the inverse closure methods perform the best, especially at higher supersaturations (0.3 %, 0.5 % and 1.0 %), where both accumulation and Aitken mode particles can activate, highlighting the importance of accounting for the size-dependent nature of aerosol composition for more accurate CCN predictions. Overall, the GMB remains well below 1.3 for κ_{MCMC}, κ_{opt} and $\kappa_{0.18}$ across all supersaturations (see Table S2), except at 0.1 %. The best agreement is observed at 0.2 % and 0.3 % supersaturations, where the GMB is around 1.1 for all methods, except for κ_{MCMC}, for which the best agreement occurs at 0.5 % and 1.0 %. These results suggest that most of the overprediction at higher supersaturations where the Aitken mode activates, can be reduced if variability in the lognormal parameters of the size distribution is also considered. However, at a supersaturation of 0.1 %, the use of size-dependent composition i.e. κ_{opt} and κ_{MCMC} does not significantly reduce the error. This suggests that the primary source of the error at this supersaturation arises from another factor – most likely, the substantial measurement uncertainty of the CCN counter at low supersaturation, as previously discussed (see Sect. 3.2).

Both inverse-closure methods reveal clear differences in aerosol composition and hygroscopicity between the Aitken and accumulation modes. The Aitken mode shows a bimodal distribution in κ, with one peak near 0.1 and another between 0.5 and 0.6, whereas that of accumulation mode is unimodal with κ values centered around 0.2–0.3. Based on this bimodality, we divided the optimized data into two groups: cases with $\kappa_{\mathrm{Aitken}} > \kappa_{\mathrm{accumulation}}$ and those with $\kappa_{\mathrm{Aitken}} < \kappa_{\mathrm{accumulation}}$. The former occurs more often in summer and is associated with a smaller Aitken-mode GMD compared to the accumulation mode. The occurrence of high κ in the Aitken mode appears to be linked – though not exclusively – to new particle formation (NPF) but limited growth. Overall, κ in the accumulation mode remains relatively stable between 0.2 and 0.3, while κ in the Aitken mode varies widely from 0.1 to 0.6. This indicates that most seasonal changes in aerosol hygroscopicity occur in the Aitken mode. In all cases, summer has comparatively more organics as biogenic secondary organic aerosols formation dominate among all aerosol sources, whereas autumn and winter show higher fractions of inorganic components due to transported and cloud-processed particles. The Aitken mode has the lowest κ values in winter, while summer features higher Aitken mode hygroscopicity (lowest accumulation mode κ) possibly due to decreasing BC content.

In the Nelder-Mead optimization, the relative difference in the median Aitken and accumulation κ is most pronounced in winter ($\sim 162\,\%$), followed by spring ($\sim 134\,\%$), autumn ($\sim 116\,\%$) and summer ($\sim 85\,\%$) reflecting seasonal shifts in aerosol sources and processes. These seasonal variations are consistent with known atmospheric processes, providing confidence in using CCN data to understand mode composition differences. The findings in this study are in line with previous research highlighting distinct differences between Aitken and accumulation mode compositions at Hyytiälä and similar environments (Hao et al., 2013). Previous studies have also demonstrated that chemical composition and hygroscopicity parameter are size-dependent (Lance et al., 2013; Ray et al., 2023) and accounting for size-dependency improves CCN predictions (Meng et al., 2014). Specifically, our results indicate that on many occasions, the accumulation mode is enriched with sulfate, while the Aitken mode is predominantly organic, in agreement with observed size-dependent chemical compositions using an Aerosol Mass Spectrometer (AMS; Allan et al., 2006). This is furthermore consistent with Mohr et al. (2019), who found that organic vapors significantly contribute to particle growth in the Aitken mode. It is notable however that all optimized compositions (κ_{opt} and κ_{MCMC}) do not resolve all the over-prediction of the CCN concentration, indicating an additional structural error in the theoretical approach or experimental uncertainties that we did not account for. If modal or size-resolved κ (in addition to just having bulk chemical composition) were available, our approach could be extended to derive more detailed size-dependent chemical composition – for example, size-dependent organic hygroscopicity – while also helping to constrain κ values by identifying those that best reproduce observed CCN concentrations.

In the future, the method applied here should be tested at other locations with varying aerosol chemical compositions – also to mitigate the inherent representativity issues related to using data from a single station. Furthermore, the approach for optimizing the closure using size-resolved composition should be compared and contrasted with other approaches, e.g. accounting for potential structural issues with the κ-Köhler model such as the treatment of the surface tension or volatility of the particle components (see e.g. Lowe et al., 2019; Heikkinen et al., 2024).

Code availability. The codes to perform inverse-closures and to generate most of the figures are available at https://github.com/rahulranjanaces/Inverse-closure.git (last access: 21 October 2025), and https://github.com/mauradewey/Modal-Aerosol-Composition (last access: 21 October 2025). These codes and also be accessed on Zenodo at https://doi.org/10.5281/zenodo.17243563 (Ranjan, 2025) and https://doi.org/10.5281/zenodo.17243685 (Dewey, 2025).

Data availability. CCN, size distribution and chemical composition data used to generate most of the figures are available at https://github.com/rahulranjanaces/Inverse-closure.git (last access: 21 October 2025) and also on Zenodo (https://doi.org/10.5281/zenodo.17243563, Ranjan, 2025; https://doi.org/10.5281/zenodo.17243685, Dewey, 2025) The raw CCN, PNSD and chemical composition data are available on Zenodo (https://doi.org/10.5281/zenodo.17277646, Ahonen et al., 2025).

Supplement. The supplement related to this article is available online at https://doi.org/10.5194/acp-25-17275-2025-supplement.

Author contributions. RR, IR, LH, DGP and AMLE conceptualized and designed the study. RR implemented the inverse-closure method with initial reference from inverse-modelling setup and guidance by DGP, and performed the majority of the calculations, and the data visualizations. MD, IR, LH, AMLE and RR conceptualized the MCMC simulation setup while MD performed all MCMC calculations and produced results. LH conducted the ACSM measurements data and provided the organo-nitrate mass fraction data, while LH and TP jointly analyzed and prepared the ACSM measurement data. AMLE and DGP actively participated in discussion meetings, providing continuous feedback on the results. LRA and PA conducted the CCN and aerosol size distribution measurements and were responsible for the calibrations. KL carried out the eBC observations, processed the data, and provided the final dataset. PB helped with initial setup and implementation of interpolation in calculation of CCN spectra. RR wrote the majority of the manuscript, with IR, LH, AMLE, DGP, KL and MD contributing significantly to the writing and revision process. All co-authors provided their feedback/comments on the manuscript. IR supervised all steps in the process.

Competing interests. At least one of the (co-)authors is a member of the editorial board of *Atmospheric Chemistry and Physics*. The peer-review process was guided by an independent editor, and the authors also have no other competing interests to declare.

Acknowledgements. We would like to thank Megan Haslum (Previously at University of Exeter) for her invaluable assistance in set-up of inverse-closure method. We are also thankful to Theodore Khadir for providing us the python implementation of the size distribution fitting algorithm. There has been use of AI tools like Grammarly (https://app.grammarly.com/, last access: 21 October 2025) and chatGPT (https://chatgpt.com/, last access: 21 October 2025) to improve the English grammar.

Financial support. This work was supported by the Knut och Alice Wallenbergs Stiftelse (grant nos. 2021.0169 and 2021.0298), the European Union's Horizon 2020 research and innovation programme via project CERTAINTY (Cloud-aERosol inTeractions & their impActs IN The earth sYstem) with grant number 101137680 and the INTEGRATE project, funded by the European Research Council Consolidator Grant (no. 865799). Göran Gustafsson foundation is also gratefully acknowledged for financial support. Daniel G. Partridge has received support from NERC (grant no. NE/W001713/1). Additional support for the SMEAR II station was provided by the University of Helsinki through ACTRIS-HY. Maura Dewey and Annica M. L. Ekman acknowledge funding from the European Union's Horizon 2020 research and innovation programme under Marie Skłodowska-Curie grant agreement no. 860100 (iMIRACLI).

The publication of this article was funded by the
Swedish Research Council, Forte, Formas, and Vinnova.

Review statement. This paper was edited by Markus Petters and reviewed by three anonymous referees.

References

Aalto, P., Hämeri, K., Becker, E. D. O., Weber, R., Salm, J., Mäkelä, J., Hoell, C., O'Dowd, C., Karlsson, H., Hansson, H.-C., Väkevä, M., Koponen, I. K., Buzorius, G., and Kulmala, M.: Physical characterization of aerosol particles during nucleation events, Tellus, Series B: Chemical and Physical Meteorology, 53, 344–358, https://doi.org/10.1034/j.1600-0889.2001.530403.x, 2001.

Aas, W., Mortier, A., Bowersox, V., Cherian, R., Faluvegi, G., Fagerli, H., Hand, J., Klimont, Z., Galy-Lacaux, C., Lehmann, C. M. B., Myhre, C. L., Myhre, G., Olivié, D., Sato, K., Quaas, J., Rao, P. S. P., Schulz, M., Shindell, D., Skeie, R. B., Stein, A., Takemura, T., Tsyro, S., Vet, R., and Xu, X.: Global and regional trends of atmospheric sulfur, Sci. Rep., 9, 953, https://doi.org/10.1038/s41598-018-37304-0, 2019.

Abdul-Razzak, H. and Ghan, S. J.: A parameterization of aerosol activation: 2. Multiple aerosol types, Journal of Geophysical Research: Atmospheres, 105, 6837–6844, https://doi.org/10.1029/1999JD901161, 2000.

Abdul-Razzak, H. and Ghan, S. J.: A parameterization of aerosol activation 3. Sectional representation, Journal of Geophysical Research: Atmospheres, 107, AAC 1-1–AAC 1-6, https://doi.org/10.1029/2001JD000483, 2002.

Ahonen, L., Petäjä, T., Heikkinen, L., Luoma, K., ranjan, rahul, and Aalto, P.: Cloud Condensation Nuclei observation data (2016–2020) for the study 'Optimizing CCN predictions through inferred modal aerosol composition – a boreal forest case study', Zenodo [data set], https://doi.org/10.5281/zenodo.17277646, 2025.

Albrecht, B. A.: Aerosols, Cloud Microphysics, and Fractional Cloudiness, Science, 245, 1227–1230, https://doi.org/10.1126/science.245.4923.1227, 1989.

Allan, J. D., Alfarra, M. R., Bower, K. N., Coe, H., Jayne, J. T., Worsnop, D. R., Aalto, P. P., Kulmala, M., Hyötyläinen, T., Cavalli, F., and Laaksonen, A.: Size and composition measurements of background aerosol and new particle growth in a Finnish forest during QUEST 2 using an Aerodyne Aerosol Mass Spectrometer, Atmos. Chem. Phys., 6, 315–327, https://doi.org/10.5194/acp-6-315-2006, 2006.

Anttila, T., Brus, D., Jaatinen, A., Hyvärinen, A.-P., Kivekäs, N., Romakkaniemi, S., Komppula, M., and Lihavainen, H.: Relationships between particles, cloud condensation nuclei and cloud droplet activation during the third Pallas Cloud Experiment, Atmos. Chem. Phys., 12, 11435–11450, https://doi.org/10.5194/acp-12-11435-2012, 2012.

Barahona, D., West, R. E. L., Stier, P., Romakkaniemi, S., Kokkola, H., and Nenes, A.: Comprehensively accounting for the effect of giant CCN in cloud activation parameterizations, Atmos. Chem. Phys., 10, 2467–2473, https://doi.org/10.5194/acp-10-2467-2010, 2010.

Bigg, E. K.: Discrepancy between observation and prediction of concentrations of cloud condensation nuclei, Atmospheric Research, 20, 81–86, https://doi.org/10.1016/0169-8095(86)90010-4, 1986.

Blichner, S. M., Yli-Juuti, T., Mielonen, T., Pöhlker, C., Holopainen, E., Heikkinen, L., Mohr, C., Artaxo, P., Carbone, S., Meller, B. B., Quaresma Dias-Júnior, C., Kulmala, M., Petäjä, T., Scott, C. E., Svenhag, C., Nieradzik, L., Sporre, M., Partridge, D. G., Tovazzi, E., Virtanen, A., Kokkola, H., and Riipinen, I.: Process-evaluation of forest aerosol-cloud-climate feedback shows clear evidence from observations and large uncertainty in models, Nat. Commun., 15, 969, https://doi.org/10.1038/s41467-024-45001-y, 2024.

Bougiatioti, A., Fountoukis, C., Kalivitis, N., Pandis, S. N., Nenes, A., and Mihalopoulos, N.: Cloud condensation nuclei measurements in the marine boundary layer of the Eastern Mediterranean: CCN closure and droplet growth kinetics, Atmos. Chem. Phys., 9, 7053–7066, https://doi.org/10.5194/acp-9-7053-2009, 2009.

Broekhuizen, K., Chang, R. Y.-W., Leaitch, W. R., Li, S.-M., and Abbatt, J. P. D.: Closure between measured and modeled cloud condensation nuclei (CCN) using size-resolved aerosol compositions in downtown Toronto, Atmos. Chem. Phys., 6, 2513–2524, https://doi.org/10.5194/acp-6-2513-2006, 2006.

Bulatovic, I., Igel, A. L., Leck, C., Heintzenberg, J., Riipinen, I., and Ekman, A. M. L.: The importance of Aitken mode aerosol particles for cloud sustenance in the summertime high Arctic – a simulation study supported by observational data, Atmos. Chem. Phys., 21, 3871–3897, https://doi.org/10.5194/acp-21-3871-2021, 2021.

Cai, M., Tan, H., Chan, C. K., Qin, Y., Xu, H., Li, F., Schurman, M. I., Liu, L., and Zhao, J.: The size-resolved cloud condensation nuclei (CCN) activity and its prediction based on aerosol hygroscopicity and composition in the Pearl Delta River (PRD) region during wintertime 2014, Atmos. Chem. Phys., 18, 16419–16437, https://doi.org/10.5194/acp-18-16419-2018, 2018.

Cerully, K. M., Raatikainen, T., Lance, S., Tkacik, D., Tiitta, P., Petäjä, T., Ehn, M., Kulmala, M., Worsnop, D. R., Laaksonen, A., Smith, J. N., and Nenes, A.: Aerosol hygroscopicity and CCN activation kinetics in a boreal forest environment during the 2007 EUCAARI campaign, Atmos. Chem. Phys., 11, 12369–12386, https://doi.org/10.5194/acp-11-12369-2011, 2011.

Chuang, P. Y., Collins, D. R., Pawlowska, H., Snider, J. R., Jonsson, H. H., Brenguier, J. L., Flagan, R. C., and Seinfeld, J. H.: CCN measurements during ACE-2 and their relationship to cloud microphysical properties, Tellus B, 52, 843–867, https://doi.org/10.1034/j.1600-0889.2000.00018.x, 2000.

Claflin, M. S. and Ziemann, P. J.: Identification and Quantitation of Aerosol Products of the Reaction of β-Pinene with NO3 Radicals and Implications for Gas- and Particle-Phase Reaction Mechanisms, J. Phys. Chem. A, 122, 3640–3652, https://doi.org/10.1021/acs.jpca.8b00692, 2018.

Clerx, M., Robinson, M., Lambert, B., Lei, C. L., Ghosh, S., Mirams, G. R., and Gavaghan, D. J.: Probabilistic Inference on Noisy Time Series (PINTS), Journal of Open Research Software, 7, https://doi.org/10.5334/jors.252, 2019.

Covert, D. S., Gras, J. L., Wiedensohler, A., and Stratmann, F.: Comparison of directly measured CCN with CCN modeled from the number-size distribution in the marine boundary layer during ACE 1 at Cape Grim, Tasmania, Journal of Geophysical Research: Atmospheres, 103, 16597–16608, https://doi.org/10.1029/98JD01093, 1998.

Croft, B., Martin, R. V., Leaitch, W. R., Burkart, J., Chang, R. Y.-W., Collins, D. B., Hayes, P. L., Hodshire, A. L., Huang, L., Kodros, J. K., Moravek, A., Mungall, E. L., Murphy, J. G., Sharma, S., Tremblay, S., Wentworth, G. R., Willis, M. D., Abbatt, J. P. D., and Pierce, J. R.: Arctic marine secondary organic aerosol contributes significantly to summertime particle size distributions in the Canadian Arctic Archipelago, Atmos. Chem. Phys., 19, 2787–2812, https://doi.org/10.5194/acp-19-2787-2019, 2019.

Cubison, M. J., Ervens, B., Feingold, G., Docherty, K. S., Ulbrich, I. M., Shields, L., Prather, K., Hering, S., and Jimenez, J. L.: The influence of chemical composition and mixing state of Los Angeles urban aerosol on CCN number and cloud properties, Atmos. Chem. Phys., 8, 5649–5667, https://doi.org/10.5194/acp-8-5649-2008, 2008.

Dewey, M.: rahulranjanaces/DREAM-MCMC: Inverse-closure using DREAM-MCMC (DREAM-MCMC), Zenodo [data set] and [code], https://doi.org/10.5281/zenodo.17243685, 2025.

Ditto, J. C., Barnes, E. B., Khare, P., Takeuchi, M., Joo, T., Bui, A. A. T., Lee-Taylor, J., Eris, G., Chen, Y., Aumont, B., Jimenez, J. L., Ng, N. L., Griffin, R. J., and Gentner, D. R.: An omnipresent diversity and variability in the chemical composition of atmospheric functionalized organic aerosol, Commun. Chem., 1, 1–13, https://doi.org/10.1038/s42004-018-0074-3, 2018.

Drinovec, L., Močnik, G., Zotter, P., Prévôt, A. S. H., Ruckstuhl, C., Coz, E., Rupakheti, M., Sciare, J., Müller, T., Wiedensohler, A., and Hansen, A. D. A.: The "dual-spot" Aethalometer: an improved measurement of aerosol black carbon with real-time loading compensation, Atmos. Meas. Tech., 8, 1965–1979, https://doi.org/10.5194/amt-8-1965-2015, 2015.

Duplessis, P., Karlsson, L., Baccarini, A., Wheeler, M., Leaitch, W. R., Svenningsson, B., Leck, C., Schmale, J., Zieger, P., and Chang, R. Y.-W.: Highly Hygroscopic Aerosols Facilitate Summer and Early-Autumn Cloud Formation at Extremely Low Concentrations Over the Central Arctic Ocean, Journal of Geophysical Research: Atmospheres, 129, e2023JD039159, https://doi.org/10.1029/2023JD039159, 2024.

El Haber, M., Gérard, V., Kleinheins, J., Ferronato, C., and Nozière, B.: Measuring the Surface Tension of Atmospheric Particles and Relevant Mixtures to Better Understand Key Atmospheric Processes, Chem. Rev., 124, 10924–10963, https://doi.org/10.1021/acs.chemrev.4c00173, 2024.

Ervens, B., Cubison, M., Andrews, E., Feingold, G., Ogren, J. A., Jimenez, J. L., DeCarlo, P., and Nenes, A.: Prediction of cloud condensation nucleus number concentration using measurements of aerosol size distributions and composition and light scattering enhancement due to humidity, Journal of Geophysical Research: Atmospheres, 112, https://doi.org/10.1029/2006JD007426, 2007.

Ervens, B., Cubison, M. J., Andrews, E., Feingold, G., Ogren, J. A., Jimenez, J. L., Quinn, P. K., Bates, T. S., Wang, J., Zhang, Q., Coe, H., Flynn, M., and Allan, J. D.: CCN predictions using simplified assumptions of organic aerosol composition and mixing state: a synthesis from six different locations, Atmos. Chem. Phys., 10, 4795–4807, https://doi.org/10.5194/acp-10-4795-2010, 2010.

Ervens, B., Sorooshian, A., Aldhaif, A. M., Shingler, T., Crosbie, E., Ziemba, L., Campuzano-Jost, P., Jimenez, J. L., and Wisthaler, A.: Is there an aerosol signature of chemical cloud processing?, Atmos. Chem. Phys., 18, 16099–16119, https://doi.org/10.5194/acp-18-16099-2018, 2018.

Farmer, D. K., Matsunaga, A., Docherty, K. S., Surratt, J. D., Seinfeld, J. H., Ziemann, P. J., and Jimenez, J. L.: Response of an aerosol mass spectrometer to organonitrates and organosulfates and implications for atmospheric chemistry, Proceedings of the National Academy of Sciences, 107, 6670–6675, https://doi.org/10.1073/pnas.0912340107, 2010.

Feijó Barreira, L. M., Duporté, G., Rönkkö, T., Parshintsev, J., Hartonen, K., Hyrsky, L., Heikkinen, E., Jussila, M., Kulmala, M., and Riekkola, M.-L.: Field measurements of biogenic volatile organic compounds in the atmosphere using solid-phase microextraction Arrow, Atmos. Meas. Tech., 11, 881–893, https://doi.org/10.5194/amt-11-881-2018, 2018.

Fountoukis, C. and Nenes, A.: Continued development of a cloud droplet formation parameterization for global climate models, Journal of Geophysical Research: Atmospheres, 110, https://doi.org/10.1029/2004JD005591, 2005.

Furutani, H., Dall'osto, M., Roberts, G. C., and Prather, K. A.: Assessment of the relative importance of atmospheric aging on CCN activity derived from field observations, Atmospheric Environment, 42, 3130–3142, https://doi.org/10.1016/j.atmosenv.2007.09.024, 2008.

Gao, F. and Han, L.: Implementing the Nelder-Mead simplex algorithm with adaptive parameters, Comput. Optim. Appl., 51, 259–277, https://doi.org/10.1007/s10589-010-9329-3, 2012.

Gelfand, A. E. and Smith, A. F. M.: Sampling-Based Approaches to Calculating Marginal Densities, Journal of the American Statistical Association, 85, 398–409, https://doi.org/10.1080/01621459.1990.10476213, 1990.

Gelman, A. and Rubin, D. B.: Inference from Iterative Simulation Using Multiple Sequences, Statistical Science, 7, 457–472, https://doi.org/10.1214/ss/1177011136, 1992.

Gunthe, S. S., King, S. M., Rose, D., Chen, Q., Roldin, P., Farmer, D. K., Jimenez, J. L., Artaxo, P., Andreae, M. O., Martin, S. T., and Pöschl, U.: Cloud condensation nuclei in pristine tropical rainforest air of Amazonia: size-resolved measurements and modeling of atmospheric aerosol composition and CCN activity, Atmos. Chem. Phys., 9, 7551–7575, https://doi.org/10.5194/acp-9-7551-2009, 2009.

Hakola, H., Hellén, H., Hemmilä, M., Rinne, J., and Kulmala, M.: In situ measurements of volatile organic compounds in a boreal forest, Atmos. Chem. Phys., 12, 11665–11678, https://doi.org/10.5194/acp-12-11665-2012, 2012.

Hallquist, M., Wenger, J. C., Baltensperger, U., Rudich, Y., Simpson, D., Claeys, M., Dommen, J., Donahue, N. M., George, C., Goldstein, A. H., Hamilton, J. F., Herrmann, H., Hoffmann, T., Iinuma, Y., Jang, M., Jenkin, M. E., Jimenez, J. L., Kiendler-Scharr, A., Maenhaut, W., McFiggans, G., Mentel, Th. F., Monod, A., Prévôt, A. S. H., Seinfeld, J. H., Surratt, J. D., Szmigielski, R., and Wildt, J.: The formation, properties and impact of secondary organic aerosol: current and emerging issues, Atmos. Chem. Phys., 9, 5155–5236, https://doi.org/10.5194/acp-9-5155-2009, 2009.

Hämeri, K., Väkevä, M., Aalto, P. P., Kulmala, M., Swietlicki, E., Zhou, J., Seidl, W., Becker, E., and O'dowd, C. D.: Hygroscopic and CCN properties of aerosol particles in boreal forests, Tellus B, 53, 359–379, https://doi.org/10.1034/j.1600-0889.2001.530404.x, 2001.

Hao, L., Romakkaniemi, S., Kortelainen, A., Jaatinen, A., Portin, H., Miettinen, P., Komppula, M., Leskinen, A., Virtanen, A., Smith, J. N., Sueper, D., Worsnop, D. R., Lehtinen, K. E. J., and Laaksonen, A.: Aerosol Chemical Composition in Cloud Events by High Resolution Time-of-Flight Aerosol Mass Spectrometry, Environ. Sci. Technol., 47, 2645–2653, https://doi.org/10.1021/es302889w, 2013.

Hegg, D. A., Covert, D. S., Jonsson, H. H., and Woods, R.: Differentiating natural and anthropogenic cloud condensation nuclei in the California coastal zone, Tellus B, 61, 669–676, https://doi.org/10.1111/j.1600-0889.2009.00435.x, 2009.

Heikkinen, L., Äijälä, M., Riva, M., Luoma, K., Dällenbach, K., Aalto, J., Aalto, P., Aliaga, D., Aurela, M., Keskinen, H., Makkonen, U., Rantala, P., Kulmala, M., Petäjä, T., Worsnop, D., and Ehn, M.: Long-term sub-micrometer aerosol chemical composition in the boreal forest: inter- and intra-annual variability, Atmos. Chem. Phys., 20, 3151–3180, https://doi.org/10.5194/acp-20-3151-2020, 2020.

Heikkinen, L., Äijälä, M., Daellenbach, K. R., Chen, G., Garmash, O., Aliaga, D., Graeffe, F., Räty, M., Luoma, K., Aalto, P., Kulmala, M., Petäjä, T., Worsnop, D., and Ehn, M.: Eight years of sub-micrometre organic aerosol composition data from the boreal forest characterized using a machine-learning approach, Atmos. Chem. Phys., 21, 10081–10109, https://doi.org/10.5194/acp-21-10081-2021, 2021.

Heikkinen, L., Partridge, D. G., Blichner, S., Huang, W., Ranjan, R., Bowen, P., Tovazzi, E., Petäjä, T., Mohr, C., and Riipinen, I.: Cloud response to co-condensation of water and organic vapors over the boreal forest, Atmos. Chem. Phys., 24, 5117–5147, https://doi.org/10.5194/acp-24-5117-2024, 2024.

Hodzic, A., Aumont, B., Knote, C., Lee-Taylor, J., Madronich, S., and Tyndall, G.: Volatility dependence of Henry's law constants of condensable organics: Application to estimate depositional loss of secondary organic aerosols, Geophysical Research Letters, 41, 4795–4804, https://doi.org/10.1002/2014GL060649, 2014.

Hoppel, W. A., Frick, G. M., and Larson, R. E.: Effect of non-precipitating clouds on the aerosol size distribution in the marine boundary layer, Geophysical Research Letters, 13, 125–128, https://doi.org/10.1029/GL013i002p00125, 1986.

Huang, W., Wu, C., Gao, L., Gramlich, Y., Haslett, S. L., Thornton, J., Lopez-Hilfiker, F. D., Lee, B. H., Song, J., Saathoff, H., Shen, X., Ramisetty, R., Tripathi, S. N., Ganguly, D., Jiang, F., Vallon, M., Schobesberger, S., Yli-Juuti, T., and Mohr, C.: Variation in chemical composition and volatility of oxygenated organic aerosol in different rural, urban, and mountain environments, Atmos. Chem. Phys., 24, 2607–2624, https://doi.org/10.5194/acp-24-2607-2024, 2024.

Hussein, T., Dal Maso, M., Petäjä, T., Koponen, I. K., Paatero, P., Aalto, P. P., Hämeri, K., and Kulmala, M.: Evaluation of an automatic algorithm for fitting the particle number size distributions, Boreal Environment Research, 10, 337–355, 2005.

Intergovernmental Panel on Climate Change (IPCC): Climate Change 2021 – The Physical Science Basis: Working Group I Contribution to the Sixth Assessment Report of the Intergovernmental Panel on Climate Change, Cambridge University Press, Cambridge, https://doi.org/10.1017/9781009157896, 2023.

Isokääntä, S., Kim, P., Mikkonen, S., Kühn, T., Kokkola, H., Yli-Juuti, T., Heikkinen, L., Luoma, K., Petäjä, T., Kipling, Z., Partridge, D., and Virtanen, A.: The effect of clouds and precipitation on the aerosol concentrations and composition in a boreal forest environment, Atmos. Chem. Phys., 22, 11823–11843, https://doi.org/10.5194/acp-22-11823-2022, 2022.

Jimenez, J. L., Canagaratna, M. R., Donahue, N. M., Prevot, A. S. H., Zhang, Q., Kroll, J. H., DeCarlo, P. F., Allan, J. D., Coe, H., Ng, N. L., Aiken, A. C., Docherty, K. S., Ulbrich, I. M., Grieshop, A. P., Robinson, A. L., Duplissy, J., Smith, J. D., Wilson, K. R., Lanz, V. A., Hueglin, C., Sun, Y. L., Tian, J., Laaksonen, A., Raatikainen, T., Rautiainen, J., Vaattovaara, P., Ehn, M., Kulmala, M., Tomlinson, J. M., Collins, D. R., Cubison, M. J., E., Dunlea, J., Huffman, J. A., Onasch, T. B., Alfarra, M. R., Williams, P. I., Bower, K., Kondo, Y., Schneider, J., Drewnick, F., Borrmann, S., Weimer, S., Demerjian, K., Salcedo, D., Cottrell, L., Griffin, R., Takami, A., Miyoshi, T., Hatakeyama, S., Shimono, A., Sun, J. Y., Zhang, Y. M., Dzepina, K., Kimmel, J. R., Sueper, D., Jayne, J. T., Herndon, S. C., Trimborn, A. M., Williams, L. R., Wood, E. C., Middlebrook, A. M., Kolb, C. E., Baltensperger, U., and Worsnop, D. R.: Evolution of Organic Aerosols in the Atmosphere, Science, 326, 1525–1529, https://doi.org/10.1126/science.1180353, 2009.

Jurányi, Z., Gysel, M., Weingartner, E., DeCarlo, P. F., Kammermann, L., and Baltensperger, U.: Measured and modelled cloud condensation nuclei number concentration at the high alpine site Jungfraujoch, Atmos. Chem. Phys., 10, 7891–7906, https://doi.org/10.5194/acp-10-7891-2010, 2010.

Khadir, T.: theodorekhadir/Particle_Size_Distribution_Log_Fit_Python: Particle_Size_Distribution_Log_Fit_Python v0.1.0 – Initial Release, Zenodo [code], https://doi.org/10.5281/zenodo.8017043, 2023.

Köhler, H.: The nucleus in and the growth of hygroscopic droplets, Trans. Faraday Soc., 32, 1152–1161, https://doi.org/10.1039/TF9363201152, 1936.

Kostenidou, E., Pathak, R. K., and Pandis, S. N.: An Algorithm for the Calculation of Secondary Organic Aerosol Density Combining AMS and SMPS Data, Aerosol Science and Technology, 41, 1002–1010, https://doi.org/10.1080/02786820701666270, 2007.

Kreidenweis, S. M., Walcek, C. J., Feingold, G., Gong, W., Jacobson, M. Z., Kim, C.-H., Liu, X., Penner, J. E., Nenes, A., and Seinfeld, J. H.: Modification of aerosol mass and size distribution due to aqueous-phase SO2 oxidation in clouds: Comparisons of several models, Journal of Geophysical Research: Atmospheres, 108, https://doi.org/10.1029/2002JD002697, 2003.

Kulmala, M. T.: Build a global Earth observatory, Nature, 553, 21–23, https://doi.org/10.1038/d41586-017-08967-y, 2018.

Kulmala, M., Nieminen, T., Nikandrova, A., Lehtipalo, K., Manninen, H. E., Kajos, M. K., Kolari, P., Lauri, A., Petaja, T., Krejci, R., Hansson, H.-C., Swietlicki, E., Lindroth, A., Christensen, T., Arneth, A., Hari, P., Back, J., Vesala, T., and Kerminen, V.-M.: CO_2-induced terrestrial climate feedback mechanism: From carbon sink to aerosol source and back, Boreal Environment Research: An International Interdisciplinary Journal, 19, 122–131, 2014.

Lance, S., Nenes, A., Medina, J., and Smith, J. N.: Mapping the Operation of the DMT Continuous Flow CCN Counter, Aerosol Science and Technology, 40, 242–254, https://doi.org/10.1080/02786820500543290, 2006.

Lance, S., Raatikainen, T., Onasch, T. B., Worsnop, D. R., Yu, X.-Y., Alexander, M. L., Stolzenburg, M. R., McMurry, P. H., Smith, J. N., and Nenes, A.: Aerosol mixing state, hygroscopic growth and cloud activation efficiency during MIRAGE 2006, Atmos. Chem. Phys., 13, 5049–5062, https://doi.org/10.5194/acp-13-5049-2013, 2013.

Leaitch, W. R.: Observations Pertaining to the Effect of Chemical Transformation in Cloud on the Anthropogenic Aerosol Size Distribution, Aerosol Science and Technology, 25, 157–173, https://doi.org/10.1080/02786829608965388, 1996.

Lehtipalo, K., Yan, C., Dada, L., Bianchi, F., Xiao, M., Wagner, R., Stolzenburg, D., Ahonen, L. R., Amorim, A., Baccarini, A., Bauer, P. S., Baumgartner, B., Bergen, A., Bernhammer, A.-K., Breitenlechner, M., Brilke, S., Buchholz, A., Mazon, S. B., Chen, D., Chen, X., Dias, A., Dommen, J., Draper, D. C., Duplissy, J., Ehn, M., Finkenzeller, H., Fischer, L., Frege, C., Fuchs, C., Garmash, O., Gordon, H., Hakala, J., He, X., Heikkinen, L., Heinritzi, M., Helm, J. C., Hofbauer, V., Hoyle, C. R., Jokinen, T., Kangasluoma, J., Kerminen, V.-M., Kim, C., Kirkby, J., Kontkanen, J., Kürten, A., Lawler, M. J., Mai, H., Mathot, S., Mauldin, R. L., Molteni, U., Nichman, L., Nie, W., Nieminen, T., Ojdanic, A., Onnela, A., Passananti, M., Petäjä, T., Piel, F., Pospisilova, V., Quéléver, L. L. J., Rissanen, M. P., Rose, C., Sarnela, N., Schallhart, S., Schuchmann, S., Sengupta, K., Simon, M., Sipilä, M., Tauber, C., Tomé, A., Tröstl, J., Väisänen, O., Vogel, A. L., Volkamer, R., Wagner, A. C., Wang, M., Weitz, L., Wimmer, D., Ye, P., Ylisirniö, A., Zha, Q., Carslaw, K. S., Curtius, J., Donahue, N. M., Flagan, R. C., Hansel, A., Riipinen, I., Virtanen, A., Winkler, P. M., Baltensperger, U., Kulmala, M., and Worsnop, D. R.: Multicomponent new particle formation from sulfuric acid, ammonia, and biogenic vapors, Science Advances, 4, eaau5363, https://doi.org/10.1126/sciadv.aau5363, 2018.

Levin, E. J. T., Prenni, A. J., Palm, B. B., Day, D. A., Campuzano-Jost, P., Winkler, P. M., Kreidenweis, S. M., DeMott, P. J., Jimenez, J. L., and Smith, J. N.: Size-resolved aerosol composition and its link to hygroscopicity at a forested site in Colorado, Atmos. Chem. Phys., 14, 2657–2667, https://doi.org/10.5194/acp-14-2657-2014, 2014.

Li, Z., Buchholz, A., and Hyttinen, N.: Predicting hygroscopic growth of organosulfur aerosol particles using COSMOtherm, Atmos. Chem. Phys., 24, 11717–11725, https://doi.org/10.5194/acp-24-11717-2024, 2024.

Liu, P., Ziemann, P. J., Kittelson, D. B., and McMurry, P. H.: Generating Particle Beams of Controlled Dimensions and Divergence: I. Theory of Particle Motion in Aerodynamic Lenses and Nozzle Expansions, Aerosol Science and Technology, 22, 293–313, https://doi.org/10.1080/02786829408959748, 1995a.

Liu, P., Ziemann, P. J., Kittelson, D. B., and McMurry, P. H.: Generating Particle Beams of Controlled Dimensions and Divergence: II. Experimental Evaluation of Particle Motion in Aerodynamic Lenses and Nozzle Expansions, Aerosol Science and Technology, 22, 314–324, https://doi.org/10.1080/02786829408959749, 1995b.

Liwendahl, M.: The seasonality and inter-annual variation of aerosol particle size distributions in boreal forest, Bachelor thesis, Institutionen för Miljövetenskap (Department of Environmental Science), Stockholm University, Degree project in Environmental Science, Bachelor Programme in Physics, Sweden, 2021.

Lowe, S., Partridge, D. G., Topping, D., and Stier, P.: Inverse modelling of Köhler theory – Part 1: A response surface analysis of CCN spectra with respect to surface-active organic species, Atmos. Chem. Phys., 16, 10941–10963, https://doi.org/10.5194/acp-16-10941-2016, 2016.

Lowe, S. J., Partridge, D. G., Davies, J. F., Wilson, K. R., Topping, D., and Riipinen, I.: Key drivers of cloud response to surface-active organics, Nat. Commun., 10, 5214, https://doi.org/10.1038/s41467-019-12982-0, 2019.

Luoma, K., Niemi, J. V., Aurela, M., Fung, P. L., Helin, A., Hussein, T., Kangas, L., Kousa, A., Rönkkö, T., Timonen, H., Virkkula, A., and Petäjä, T.: Spatiotemporal variation and trends in equivalent black carbon in the Helsinki metropolitan area in Finland, Atmospheric Chemistry and Physics, 21, 1173–1189, https://doi.org/10.5194/acp-21-1173-2021, 2021.

Martin, M., Chang, R. Y.-W., Sierau, B., Sjogren, S., Swietlicki, E., Abbatt, J. P. D., Leck, C., and Lohmann, U.: Cloud condensation nuclei closure study on summer arctic aerosol, Atmos. Chem. Phys., 11, 11335–11350, https://doi.org/10.5194/acp-11-11335-2011, 2011.

Massling, A., Lange, R., Pernov, J. B., Gosewinkel, U., Sørensen, L.-L., and Skov, H.: Measurement report: High Arctic aerosol hygroscopicity at sub- and supersaturated conditions during spring and summer, Atmos. Chem. Phys., 23, 4931–4953, https://doi.org/10.5194/acp-23-4931-2023, 2023.

Meng, J. W., Yeung, M. C., Li, Y. J., Lee, B. Y. L., and Chan, C. K.: Size-resolved cloud condensation nuclei (CCN) activity and closure analysis at the HKUST Supersite in Hong Kong, Atmos. Chem. Phys., 14, 10267–10282, https://doi.org/10.5194/acp-14-10267-2014, 2014.

Merikanto, J., Spracklen, D. V., Mann, G. W., Pickering, S. J., and Carslaw, K. S.: Impact of nucleation on global CCN, Atmos. Chem. Phys., 9, 8601–8616, https://doi.org/10.5194/acp-9-8601-2009, 2009.

Metropolis, N., Rosenbluth, A. W., Rosenbluth, M. N., Teller, A. H., and Teller, E.: Equation of State Calculations by Fast Computing Machines, J. Chem. Phys., 21, 1087–1092, https://doi.org/10.1063/1.1699114, 1953.

Mohr, C., Thornton, J. A., Heitto, A., Lopez-Hilfiker, F. D., Lutz, A., Riipinen, I., Hong, J., Donahue, N. M., Hallquist, M., Petäjä, T., Kulmala, M., and Yli-Juuti, T.: Molecular identification of organic vapors driving atmospheric nanoparticle growth, Nat. Commun., 10, 4442, https://doi.org/10.1038/s41467-019-12473-2, 2019.

Morales Betancourt, R. and Nenes, A.: Droplet activation parameterization: the population-splitting concept revisited, Geosci. Model Dev., 7, 2345–2357, https://doi.org/10.5194/gmd-7-2345-2014, 2014.

Nenes, A. and Seinfeld, J. H.: Parameterization of cloud droplet formation in global climate models, Journal of Geophysical Research: Atmospheres, 108, https://doi.org/10.1029/2002JD002911, 2003.

Nenes, A., Pandis, S. N., and Pilinis, C.: ISORROPIA: A new thermodynamic equilibrium model for multiphase multicomponent inorganic aerosols, Aquatic Geochemistry, 4, 123–152, https://doi.org/10.1023/A:1009604003981, 1998.

Nenes, A., Pandis, S. N., and Pilinis, C.: Continued development and testing of a new thermodynamic aerosol module for urban and regional air quality models, Atmospheric Environment, 33, 1553–1560, https://doi.org/10.1016/S1352-2310(98)00352-5, 1999.

Ng, N. L., Herndon, S. C., Trimborn, A., Canagaratna, M. R., Croteau, P. L., Onasch, T. B., Sueper, D., Worsnop, D. R., Zhang, Q., Sun, Y. L., and Jayne, J. T.: An Aerosol Chemical Speciation Monitor (ACSM) for Routine Monitoring of the Composition and Mass Concentrations of Ambient Aerosol, Aerosol Science and Technology, 45, 780–794, https://doi.org/10.1080/02786826.2011.560211, 2011.

Nieminen, T., Asmi, A., Dal Maso, M., Aalto, P., Keronen, P., Petäjä, T., Kulmala, M., and Kerminen, V.-M.: Trends in atmospheric new-particle formation: 16 years of observations in a boreal-forest environment, Boreal Environment Research, 19, 191–214, 2014.

Nozière, B., Kalberer, M., Claeys, M., Allan, J., D'Anna, B., Decesari, S., Finessi, E., Glasius, M., Grgić, I., Hamilton, J. F., Hoffmann, T., Iinuma, Y., Jaoui, M., Kahnt, A., Kampf, C. J., Kourtchev, I., Maenhaut, W., Marsden, N., Saarikoski, S., Schnelle-Kreis, J., Surratt, J. D., Szidat, S., Szmigielski, R., and Wisthaler, A.: The Molecular Identification of Organic Compounds in the Atmosphere: State of the Art and Challenges, Chem. Rev., 115, 3919–3983, https://doi.org/10.1021/cr5003485, 2015.

Paasonen, P., Asmi, A., Petäjä, T., Kajos, M. K., Äijälä, M., Junninen, H., Holst, T., Abbatt, J. P. D., Arneth, A., Birmili, W., van der Gon, H. D., Hamed, A., Hoffer, A., Laakso, L., Laaksonen, A., Richard Leaitch, W., Plass-Dülmer, C., Pryor, S. C., Räisänen, P., Swietlicki, E., Wiedensohler, A., Worsnop, D. R., Kerminen, V.-M., and Kulmala, M.: Warming-induced increase in aerosol number concentration likely to moderate climate change, Nature Geosci., 6, 438–442, https://doi.org/10.1038/ngeo1800, 2013.

Paramonov, M., Aalto, P. P., Asmi, A., Prisle, N., Kerminen, V.-M., Kulmala, M., and Petäjä, T.: The analysis of size-segregated cloud condensation nuclei counter (CCNC) data and its implications for cloud droplet activation, Atmos. Chem. Phys., 13, 10285–10301, https://doi.org/10.5194/acp-13-10285-2013, 2013.

Paramonov, M., Kerminen, V.-M., Gysel, M., Aalto, P. P., Andreae, M. O., Asmi, E., Baltensperger, U., Bougiatioti, A., Brus, D., Frank, G. P., Good, N., Gunthe, S. S., Hao, L., Irwin, M., Jaatinen, A., Jurányi, Z., King, S. M., Kortelainen, A., Kristensson, A., Lihavainen, H., Kulmala, M., Lohmann, U., Martin, S. T., McFiggans, G., Mihalopoulos, N., Nenes, A., O'Dowd, C. D., Ovadnevaite, J., Petäjä, T., Pöschl, U., Roberts, G. C., Rose, D., Svenningsson, B., Swietlicki, E., Weingartner, E., Whitehead, J., Wiedensohler, A., Wittbom, C., and Sierau, B.: A synthesis of cloud condensation nuclei counter (CCNC) measurements within the EUCAARI network, Atmos. Chem. Phys., 15, 12211–12229, https://doi.org/10.5194/acp-15-12211-2015, 2015.

Park, K., Kittelson, D. B., and McMurry, P. H.: Structural Properties of Diesel Exhaust Particles Measured by Transmission Electron Microscopy (TEM): Relationships to Particle Mass and Mobility, Aerosol Science and Technology, 38, 881–889, https://doi.org/10.1080/027868290505189, 2004.

Partridge, D. G., Vrugt, J. A., Tunved, P., Ekman, A. M. L., Gorea, D., and Sorooshian, A.: Inverse modeling of cloud-aerosol interactions – Part 1: Detailed response surface analysis, Atmos. Chem. Phys., 11, 7269–7287, https://doi.org/10.5194/acp-11-7269-2011, 2011.

Partridge, D. G., Vrugt, J. A., Tunved, P., Ekman, A. M. L., Struthers, H., and Sorooshian, A.: Inverse modelling of cloud-aerosol interactions – Part 2: Sensitivity tests on liquid phase clouds using a Markov chain Monte Carlo based simulation approach, Atmos. Chem. Phys., 12, 2823–2847, https://doi.org/10.5194/acp-12-2823-2012, 2012.

Patokoski, J., Ruuskanen, T. M., Kajos, M. K., Taipale, R., Rantala, P., Aalto, J., Ryyppö, T., Nieminen, T., Hakola, H., and Rinne, J.: Sources of long-lived atmospheric VOCs at the rural boreal forest site, SMEAR II, Atmos. Chem. Phys., 15, 13413–13432, https://doi.org/10.5194/acp-15-13413-2015, 2015.

Petters, M. D. and Kreidenweis, S. M.: A single parameter representation of hygroscopic growth and cloud condensation nucleus activity, Atmos. Chem. Phys., 7, 1961–1971, https://doi.org/10.5194/acp-7-1961-2007, 2007.

Pierce, J. R., Leaitch, W. R., Liggio, J., Westervelt, D. M., Wainwright, C. D., Abbatt, J. P. D., Ahlm, L., Al-Basheer, W., Cziczo, D. J., Hayden, K. L., Lee, A. K. Y., Li, S.-M., Russell, L. M., Sjostedt, S. J., Strawbridge, K. B., Travis, M., Vlasenko, A., Wentzell, J. J. B., Wiebe, H. A., Wong, J. P. S., and Macdonald, A. M.: Nucleation and condensational growth to CCN sizes during a sustained pristine biogenic SOA event in a forested mountain valley, Atmos. Chem. Phys., 12, 3147–3163, https://doi.org/10.5194/acp-12-3147-2012, 2012.

Pöhlker, M. L., Zhang, M., Campos Braga, R., Krüger, O. O., Pöschl, U., and Ervens, B.: Aitken mode particles as CCN in aerosol- and updraft-sensitive regimes of cloud droplet formation, Atmos. Chem. Phys., 21, 11723–11740, https://doi.org/10.5194/acp-21-11723-2021, 2021.

Pöhlker, M. L., Pöhlker, C., Quaas, J., Mülmenstädt, J., Pozzer, A., Andreae, M. O., Artaxo, P., Block, K., Coe, H., Ervens, B., Gallimore, P., Gaston, C. J., Gunthe, S. S., Henning, S., Herrmann, H., Krüger, O. O., McFiggans, G., Poulain, L., Raj, S.

S., Reyes-Villegas, E., Royer, H. M., Walter, D., Wang, Y., and Pöschl, U.: Global organic and inorganic aerosol hygroscopicity and its effect on radiative forcing, Nat. Commun., 14, 6139, https://doi.org/10.1038/s41467-023-41695-8, 2023.

Pruppacher, H. R. and Klett, J. D.: Microphysics of Clouds and Precipitation, Springer Netherlands, Dordrecht, https://doi.org/10.1007/978-0-306-48100-0, 2010.

Qiao, X., Yan, C., Li, X., Guo, Y., Yin, R., Deng, C., Li, C., Nie, W., Wang, M., Cai, R., Huang, D., Wang, Z., Yao, L., Worsnop, D. R., Bianchi, F., Liu, Y., Donahue, N. M., Kulmala, M., and Jiang, J.: Contribution of Atmospheric Oxygenated Organic Compounds to Particle Growth in an Urban Environment, Environ. Sci. Technol., 55, 13646–13656, https://doi.org/10.1021/acs.est.1c02095, 2021.

Quinn, P. K., Bates, T. S., Coffman, D. J., and Covert, D. S.: Influence of particle size and chemistry on the cloud nucleating properties of aerosols, Atmos. Chem. Phys., 8, 1029–1042, https://doi.org/10.5194/acp-8-1029-2008, 2008.

Ranjan, R.: rahulranjanaces/Inverse-closure: inverse-closure (version 0), Zenodo [data set and code] https://doi.org/10.5281/zenodo.17243563, 2025.

Rastak, N., Pajunoja, A., Acosta Navarro, J. C., Ma, J., Song, M., Partridge, D. G., Kirkevåg, A., Leong, Y., Hu, W. W., Taylor, N. F., Lambe, A., Cerully, K., Bougiatioti, A., Liu, P., Krejci, R., Petäjä, T., Percival, C., Davidovits, P., Worsnop, D. R., Ekman, A. M. L., Nenes, A., Martin, S., Jimenez, J. L., Collins, D. R., Topping, D. o., Bertram, A. K., Zuend, A., Virtanen, A., and Riipinen, I.: Microphysical explanation of the RH-dependent water affinity of biogenic organic aerosol and its importance for climate, Geophysical Research Letters, 44, 5167–5177, https://doi.org/10.1002/2017GL073056, 2017.

Ray, A., Pandithurai, G., Mukherjee, S., Kumar, V. A., Hazra, A., Patil, R. D., and Waghmare, V.: Seasonal variability in size-resolved hygroscopicity of sub-micron aerosols over the Western Ghats, India: Closure and parameterization, Science of The Total Environment, 869, 161753, https://doi.org/10.1016/j.scitotenv.2023.161753, 2023.

Rejano, F., Casans, A., Via, M., Casquero-Vera, J. A., Castillo, S., Lyamani, H., Cazorla, A., Andrews, E., Pérez-Ramírez, D., Alastuey, A., Gómez-Moreno, F. J., Alados-Arboledas, L., Olmo, F. J., and Titos, G.: CCN estimations at a high-altitude remote site: role of organic aerosol variability and hygroscopicity, Atmos. Chem. Phys., 24, 13865–13888, https://doi.org/10.5194/acp-24-13865-2024, 2024.

Reutter, P., Su, H., Trentmann, J., Simmel, M., Rose, D., Gunthe, S. S., Wernli, H., Andreae, M. O., and Pöschl, U.: Aerosol- and updraft-limited regimes of cloud droplet formation: influence of particle number, size and hygroscopicity on the activation of cloud condensation nuclei (CCN), Atmos. Chem. Phys., 9, 7067–7080, https://doi.org/10.5194/acp-9-7067-2009, 2009.

Riipinen, I., Pierce, J. R., Yli-Juuti, T., Nieminen, T., Häkkinen, S., Ehn, M., Junninen, H., Lehtipalo, K., Petäjä, T., Slowik, J., Chang, R., Shantz, N. C., Abbatt, J., Leaitch, W. R., Kerminen, V.-M., Worsnop, D. R., Pandis, S. N., Donahue, N. M., and Kulmala, M.: Organic condensation: a vital link connecting aerosol formation to cloud condensation nuclei (CCN) concentrations, Atmos. Chem. Phys., 11, 3865–3878, https://doi.org/10.5194/acp-11-3865-2011, 2011.

Rissman, T. A., VanReken, T. M., Wang, J., Gasparini, R., Collins, D. R., Jonsson, H. H., Brechtel, F. J., Flagan, R. C., and Seinfeld, J. H.: Characterization of ambient aerosol from measurements of cloud condensation nuclei during the 2003 Atmospheric Radiation Measurement Aerosol Intensive Observational Period at the Southern Great Plains site in Oklahoma, Journal of Geophysical Research: Atmospheres, 111, https://doi.org/10.1029/2004JD005695, 2006.

Riuttanen, L., Hulkkonen, M., Dal Maso, M., Junninen, H., and Kulmala, M.: Trajectory analysis of atmospheric transport of fine particles, SO_2, NO_x and O_3 to the SMEAR II station in Finland in 1996–2008, Atmos. Chem. Phys., 13, 2153–2164, https://doi.org/10.5194/acp-13-2153-2013, 2013.

Riva, M., Chen, Y., Zhang, Y., Lei, Z., Olson, N. E., Boyer, H. C., Narayan, S., Yee, L. D., Green, H. S., Cui, T., Zhang, Z., Baumann, K., Fort, M., Edgerton, E., Budisulistiorini, S. H., Rose, C. A., Ribeiro, I. O., e Oliveira, R. L., dos Santos, E. O., Machado, C. M. D., Szopa, S., Zhao, Y., Alves, E. G., de Sá, S. S., Hu, W., Knipping, E. M., Shaw, S. L., Duvoisin Junior, S., de Souza, R. A. F., Palm, B. B., Jimenez, J.-L., Glasius, M., Goldstein, A. H., Pye, H. O. T., Gold, A., Turpin, B. J., Vizuete, W., Martin, S. T., Thornton, J. A., Dutcher, C. S., Ault, A. P., and Surratt, J. D.: Increasing Isoprene Epoxydiol-to-Inorganic Sulfate Aerosol Ratio Results in Extensive Conversion of Inorganic Sulfate to Organosulfur Forms: Implications for Aerosol Physicochemical Properties, Environ. Sci. Technol., 53, 8682–8694, https://doi.org/10.1021/acs.est.9b01019, 2019.

Roberts, G., Mauger, G., Hadley, O., and Ramanathan, V.: North American and Asian aerosols over the eastern Pacific Ocean and their role in regulating cloud condensation nuclei, Journal of Geophysical Research: Atmospheres, 111, https://doi.org/10.1029/2005JD006661, 2006.

Roberts, G. C. and Nenes, A.: A Continuous-Flow Streamwise Thermal-Gradient CCN Chamber for Atmospheric Measurements, Aerosol Science and Technology, 39, 206–221, https://doi.org/10.1080/027868290913988, 2005.

Robinson, A. L., Donahue, N. M., Shrivastava, M. K., Weitkamp, E. A., Sage, A. M., Grieshop, A. P., Lane, T. E., Pierce, J. R., and Pandis, S. N.: Rethinking Organic Aerosols: Semivolatile Emissions and Photochemical Aging, Science, 315, 1259–1262, https://doi.org/10.1126/science.1133061, 2007.

Roelofs, G.-J. a N., Lelieveld, J., and Ganzeveld, L.: Simulation of global sulfate distribution and the influence on effective cloud drop radii with a coupled photochemistry sulfur cycle model, Tellus B, 50, 224–242, https://doi.org/10.1034/j.1600-0889.1998.t01-2-00002.x, 1998.

Rogers, R. R. and Yau, M. K.: A Short Course in Cloud Physics, 3rd edn., Butterworth–Heinemann, ISBN 978-0-7506-3215-7, 1989.

Rose, D., Gunthe, S. S., Mikhailov, E., Frank, G. P., Dusek, U., Andreae, M. O., and Pöschl, U.: Calibration and measurement uncertainties of a continuous-flow cloud condensation nuclei counter (DMT-CCNC): CCN activation of ammonium sulfate and sodium chloride aerosol particles in theory and experiment, Atmos. Chem. Phys., 8, 1153–1179, https://doi.org/10.5194/acp-8-1153-2008, 2008.

Saliba, G., Sanchez, K. J., Russell, L. M., Twohy, C. H., Roberts, G. C., Lewis, S., Dedrick, J., McCluskey, C. S., Moore, K., DeMott, P. J., and Toohey, D. W.: Organic composition of three different size ranges of aerosol particles over the Southern Ocean, Aerosol Science and Technology, 55, 268–288, https://doi.org/10.1080/02786826.2020.1845296, 2020.

Schmale, J., Henning, S., Decesari, S., Henzing, B., Keskinen, H., Sellegri, K., Ovadnevaite, J., Pöhlker, M. L., Brito, J., Bougiatioti, A., Kristensson, A., Kalivitis, N., Stavroulas, I., Carbone, S., Jefferson, A., Park, M., Schlag, P., Iwamoto, Y., Aalto, P., Äijälä, M., Bukowiecki, N., Ehn, M., Frank, G., Fröhlich, R., Frumau, A., Herrmann, E., Herrmann, H., Holzinger, R., Kos, G., Kulmala, M., Mihalopoulos, N., Nenes, A., O'Dowd, C., Petäjä, T., Picard, D., Pöhlker, C., Pöschl, U., Poulain, L., Prévôt, A. S. H., Swietlicki, E., Andreae, M. O., Artaxo, P., Wiedensohler, A., Ogren, J., Matsuki, A., Yum, S. S., Stratmann, F., Baltensperger, U., and Gysel, M.: Long-term cloud condensation nuclei number concentration, particle number size distribution and chemical composition measurements at regionally representative observatories, Atmos. Chem. Phys., 18, 2853–2881, https://doi.org/10.5194/acp-18-2853-2018, 2018.

Seinfeld, J. H., Bretherton, C., Carslaw, K. S., Coe, H., DeMott, P. J., Dunlea, E. J., Feingold, G., Ghan, S., Guenther, A. B., Kahn, R., Kraucunas, I., Kreidenweis, S. M., Molina, M. J., Nenes, A., Penner, J. E., Prather, K. A., Ramanathan, V., Ramaswamy, V., Rasch, P. J., Ravishankara, A. R., Rosenfeld, D., Stephens, G., and Wood, R.: Improving our fundamental understanding of the role of aerosol-cloud interactions in the climate system, Proceedings of the National Academy of Sciences, 113, 5781–5790, https://doi.org/10.1073/pnas.1514043113, 2016.

Siegel, K., Neuberger, A., Karlsson, L., Zieger, P., Mattsson, F., Duplessis, P., Dada, L., Daellenbach, K., Schmale, J., Baccarini, A., Krejci, R., Svenningsson, B., Chang, R., Ekman, A. M. L., Riipinen, I., and Mohr, C.: Using Novel Molecular-Level Chemical Composition Observations of High Arctic Organic Aerosol for Predictions of Cloud Condensation Nuclei, Environ. Sci. Technol., 56, 13888–13899, https://doi.org/10.1021/acs.est.2c02162, 2022.

Sihto, S.-L., Mikkilä, J., Vanhanen, J., Ehn, M., Liao, L., Lehtipalo, K., Aalto, P. P., Duplissy, J., Petäjä, T., Kerminen, V.-M., Boy, M., and Kulmala, M.: Seasonal variation of CCN concentrations and aerosol activation properties in boreal forest, Atmos. Chem. Phys., 11, 13269–13285, https://doi.org/10.5194/acp-11-13269-2011, 2011.

Simpson, E., Connolly, P., and McFiggans, G.: An investigation into the performance of four cloud droplet activation parameterisations, Geosci. Model Dev., 7, 1535–1542, https://doi.org/10.5194/gmd-7-1535-2014, 2014.

Spitieri, C., Gini, M., Gysel-Beer, M., and Eleftheriadis, K.: Annual cycle of hygroscopic properties and mixing state of the suburban aerosol in Athens, Greece, Atmos. Chem. Phys., 23, 235–249, https://doi.org/10.5194/acp-23-235-2023, 2023.

Stokes, R. H. and Robinson, R. A.: Interactions in aqueous nonelectrolyte solutions. I. Solute-solvent equilibria, J. Phys. Chem., 70, 2126–2130, 1966.

Stroud, C. A., Nenes, A., Jimenez, J. L., DeCarlo, P. F., Huffman, J. A., Bruintjes, R., Nemitz, E., Delia, A. E., Toohey, D. W., Guenther, A. B., and Nandi, S.: Cloud Activating Properties of Aerosol Observed during CELTIC, Journal of the Atmospheric Sciences, 64, 441–459, https://doi.org/10.1175/JAS3843.1, 2007.

Timonen, H., Saarikoski, S., Tolonen-Kivimäki, O., Aurela, M., Saarnio, K., Petäjä, T., Aalto, P. P., Kulmala, M., Pakkanen, T., and Hillamo, R.: Size distributions, sources and source areas of water-soluble organic carbon in urban background air, Atmos. Chem. Phys., 8, 5635–5647, https://doi.org/10.5194/acp-8-5635-2008, 2008.

Topping, D. O., McFiggans, G. B., and Coe, H.: A curved multi-component aerosol hygroscopicity model framework: Part 1 – Inorganic compounds, Atmos. Chem. Phys., 5, 1205–1222, https://doi.org/10.5194/acp-5-1205-2005, 2005.

Tunved, P., Hansson, H.-C., Kerminen, V.-M., Ström, J., Maso, M. D., Lihavainen, H., Viisanen, Y., Aalto, P. P., Komppula, M., and Kulmala, M.: High Natural Aerosol Loading over Boreal Forests, Science, 312, 261–263, https://doi.org/10.1126/science.1123052, 2006.

Twomey, S.: Pollution and the planetary albedo, Atmospheric Environment, 8, 1251–1256, https://doi.org/10.1016/0004-6981(74)90004-3, 1974.

Virkkula, A., Mäkelä, T., Hillamo, R., Yli-Tuomi, T., Hirsikko, A., Hämeri, K., and Koponen, I. K.: A Simple Procedure for Correcting Loading Effects of Aethalometer Data, Journal of the Air & Waste Management Association, 57, 1214–1222, https://doi.org/10.3155/1047-3289.57.10.1214, 2007.

Vrugt, J. A., ter Braak, C. J. F., Diks, C. G. H., Robinson, B. A., Hyman, J. M., and Higdon, D.: Accelerating Markov Chain Monte Carlo Simulation by Differential Evolution with Self-Adaptive Randomized Subspace Sampling, International Journal of Nonlinear Sciences and Numerical Simulation, 10, 273–290, https://doi.org/10.1515/IJNSNS.2009.10.3.273, 2009.

Wang, J., Cubison, M. J., Aiken, A. C., Jimenez, J. L., and Collins, D. R.: The importance of aerosol mixing state and size-resolved composition on CCN concentration and the variation of the importance with atmospheric aging of aerosols, Atmos. Chem. Phys., 10, 7267–7283, https://doi.org/10.5194/acp-10-7267-2010, 2010.

Weingartner, E., Burtscher, H., and Baltensperger, U.: Hygroscopic properties of carbon and diesel soot particles, Atmospheric Environment, 31, 2311–2327, https://doi.org/10.1016/S1352-2310(97)00023-X, 1997.

Williams, J., Crowley, J., Fischer, H., Harder, H., Martinez, M., Petäjä, T., Rinne, J., Bäck, J., Boy, M., Dal Maso, M., Hakala, J., Kajos, M., Keronen, P., Rantala, P., Aalto, J., Aaltonen, H., Paatero, J., Vesala, T., Hakola, H., Levula, J., Pohja, T., Herrmann, F., Auld, J., Mesarchaki, E., Song, W., Yassaa, N., Nölscher, A., Johnson, A. M., Custer, T., Sinha, V., Thieser, J., Pouvesle, N., Taraborrelli, D., Tang, M. J., Bozem, H., Hosaynali-Beygi, Z., Axinte, R., Oswald, R., Novelli, A., Kubistin, D., Hens, K., Javed, U., Trawny, K., Breitenberger, C., Hidalgo, P. J., Ebben, C. J., Geiger, F. M., Corrigan, A. L., Russell, L. M., Ouwersloot, H. G., Vilà-Guerau de Arellano, J., Ganzeveld, L., Vogel, A., Beck, M., Bayerle, A., Kampf, C. J., Bertelmann, M., Köllner, F., Hoffmann, T., Valverde, J., González, D., Riekkola, M.-L., Kulmala, M., and Lelieveld, J.: The summertime Boreal forest field measurement intensive (HUMPPA-COPEC-2010): an overview of meteorological and chemical influences, Atmos. Chem. Phys., 11, 10599–10618, https://doi.org/10.5194/acp-11-10599-2011, 2011.

Wonaschuetz, A., Sorooshian, A., Ervens, B., Chuang, P. Y., Feingold, G., Murphy, S. M., de Gouw, J., Warneke, C., and Jonsson, H. H.: Aerosol and gas re-distribution by shallow cumulus clouds: An investigation using airborne measurements, Journal of Geophysical Research: Atmospheres, 117, https://doi.org/10.1029/2012JD018089, 2012.

Wu, Z. J., Zheng, J., Shang, D. J., Du, Z. F., Wu, Y. S., Zeng, L. M., Wiedensohler, A., and Hu, M.: Particle hygroscopicity and its link to chemical composition in the urban atmosphere of Beijing, China, during summertime, Atmos. Chem. Phys., 16, 1123–1138, https://doi.org/10.5194/acp-16-1123-2016, 2016.

Yan, C., Dada, L., Rose, C., Jokinen, T., Nie, W., Schobesberger, S., Junninen, H., Lehtipalo, K., Sarnela, N., Makkonen, U., Garmash, O., Wang, Y., Zha, Q., Paasonen, P., Bianchi, F., Sipilä, M., Ehn, M., Petäjä, T., Kerminen, V.-M., Worsnop, D. R., and Kulmala, M.: The role of H_2SO_4-NH_3 anion clusters in ion-induced aerosol nucleation mechanisms in the boreal forest, Atmos. Chem. Phys., 18, 13231–13243, https://doi.org/10.5194/acp-18-13231-2018, 2018.

Ye, J., Gordon, C. A., and Chan, A. W. H.: Enhancement in Secondary Organic Aerosol Formation in the Presence of Preexisting Organic Particle, Environ. Sci. Technol., 50, 3572–3579, https://doi.org/10.1021/acs.est.5b05512, 2016.

Yli-Juuti, T., Mielonen, T., Heikkinen, L., Arola, A., Ehn, M., Isokääntä, S., Keskinen, H.-M., Kulmala, M., Laakso, A., Lipponen, A., Luoma, K., Mikkonen, S., Nieminen, T., Paasonen, P., Petäjä, T., Romakkaniemi, S., Tonttila, J., Kokkola, H., and Virtanen, A.: Significance of the organic aerosol driven climate feedback in the boreal area, Nat. Commun., 12, 5637, https://doi.org/10.1038/s41467-021-25850-7, 2021.

Yttri, K. E., Simpson, D., Nøjgaard, J. K., Kristensen, K., Genberg, J., Stenström, K., Swietlicki, E., Hillamo, R., Aurela, M., Bauer, H., Offenberg, J. H., Jaoui, M., Dye, C., Eckhardt, S., Burkhart, J. F., Stohl, A., and Glasius, M.: Source apportionment of the summer time carbonaceous aerosol at Nordic rural background sites, Atmos. Chem. Phys., 11, 13339–13357, https://doi.org/10.5194/acp-11-13339-2011, 2011.

Zhang, Q., Jimenez, J. L., Canagaratna, M. R., Allan, J. D., Coe, H., Ulbrich, I., Alfarra, M. R., Takami, A., Middlebrook, A. M., Sun, Y. L., Dzepina, K., Dunlea, E., Docherty, K., DeCarlo, P. F., Salcedo, D., Onasch, T., Jayne, J. T., Miyoshi, T., Shimono, A., Hatakeyama, S., Takegawa, N., Kondo, Y., Schneider, J., Drewnick, F., Borrmann, S., Weimer, S., Demerjian, K., Williams, P., Bower, K., Bahreini, R., Cottrell, L., Griffin, R. J., Rautiainen, J., Sun, J. Y., Zhang, Y. M., and Worsnop, D. R.: Ubiquity and dominance of oxygenated species in organic aerosols in anthropogenically-influenced Northern Hemisphere midlatitudes, Geophysical Research Letters, 34, https://doi.org/10.1029/2007GL029979, 2007.

Zhang, Y., Seigneur, C., Seinfeld, J. H., Jacobson, M., Clegg, S. L., and Binkowski, F. S.: A comparative review of inorganic aerosol thermodynamic equilibrium modules: similarities, differences, and their likely causes, Atmospheric Environment, 34, 117–137, https://doi.org/10.1016/S1352-2310(99)00236-8, 2000.

Zheng, G., Kuang, C., Uin, J., Watson, T., and Wang, J.: Large contribution of organics to condensational growth and formation of cloud condensation nuclei (CCN) in the remote marine boundary layer, Atmos. Chem. Phys., 20, 12515–12525, https://doi.org/10.5194/acp-20-12515-2020, 2020.